Emergence of a senescent and inflammatory pulmonary CD4$^+$ T cell population prior to lung allograft failure

Sajad Moshkelgosha[1], Liran Levy[1,2], Shahideh Safavi[1,3], Sumiha Karunagaran[1], Gavin Wilson[1], Benjamin Renaud-Picard[1,4], Goodness Madu[1], Rashi Ramchandani[1], Jillian Oliver[1], Tatsuaki Watanabe[1,5], Ke Fan Bei[1], Betty Joe[1], Qixuan Li[6], Ella Huszti[6], May Cheung[1], David Hedley[7], Jonathan Yeung[1,8,9], Shaf Keshavjee[1,8,9], Tereza Martinu[1,8,10], Stephen Juvet[1,8,10]

1. Toronto General Hospital Research Institute, University Health Network, Toronto, ON
2. Sheba Medical Center, Sackler School of Medicine, Tel-Aviv University, Tel-Aviv, Israel
3. Barts Health NHS Trust, London, UK
4. Nouvel Hôpital Civil, Strasbourg, France
5. Department of Thoracic Surggery, Institute of Development, Aging and Cancer, Tohoku University, Sendai, Japan
6. Biostatistics Department, University Health Network, Toronto, ON
7. Division of Medical Oncology, Department of Medicine, University of Toronto
8. Toronto Lung Transplant Program, Ajmera Transplant Centre, University Health Network, Toronto, ON
9. Division of Thoracic Surgery, Department of Surgery, University of Toronto, Toronto, ON
10. Division of Respirology, Department of Medicine, University of Toronto, Toronto, ON

Address of Corresponding Author:
Stephen Juvet, MD, PhD
Toronto General Hospital: University Health Network (UHN)
200 Elizabeth St., Rm 11 PMB 126
Toronto, Ontario, M5G 2C4
EMAIL: stephen.juvet@uhn.ca
TEL: (416) 340-4800 - ext: 8178

Acknowledgments

The authors wish to thank Martin Oberle, Marcelo Cuesta, Iva Avramov and other members of the Toronto Lung Transplant Program Biobank for their assistance with sample procurement and storage. We also thank Dr. Cynthia Guidos and Dr. Dariush Davani for their critical input on the design of mass cytometry experiments. We also wish to thank Dr. Sarah Crome and Sarah Colpitts for their assistance and advice in planning CITE-Seq experiments.

This work was funded by Cystic Fibrosis Foundation grants JUVET18AB0 and JUVET23G0 (to S.J.), and MARTIN18I0 (to T.M. and S.J.) by an International Society for Heart and Lung Transplantation Norman Shumway Career Development Award (to S.J.), by a Canadian Society of Transplantation Research Training Award (to S.M.) and by the University Health Network Foundation.

Abbreviations:

ALAD: Acute lung allograft dysfunction

CLAD: Chronic lung allograft dysfunction

LT: Lung transplantation

BAL: Bronchoalveolar lavage

IMC: Imaging mass cytometry

tSNE: T-distributed stochastic neighbor embedding

CyTOF: Cytometry by Time of Flight

CITE-seq: Cellular indexing of transcriptomes and epitopes

Tph: peripheral helper T

FEV1: Forced expiratory volume in one second

TLTP: Toronto lung transplant program

GLMM: Generalized linear mixed model

ROC: Receiver-operating characteristic

DSA: Donor specific antibodies

HR: Hazard radio

CMV: Cytomegalovirus

ADT: Antibody derived tags

RICD: Restimulation induced cell death

Disclosure

Sajad Moshkelgosha, Shaf Keshavjee and Stephen Juvet have filed US patent US63/460,274 in relation to the work in this manuscript.

Abstract

Lung transplantation is a life-saving therapy for end-stage pulmonary disease, but its long-term outlook is poor due to a high incidence of chronic lung allograft dysfunction (CLAD). CLAD results from alloimmune-mediated progressive fibrosis and culminates in death or the need for re-transplantation after a median of 6 years. Existing immunosuppression fails to prevent CLAD, suggesting the existence of alloimmune pathways resistant to these drugs. Here, we used mass cytometry to identify cell populations enriched in the bronchoalveolar lavage (BAL) of patients with subsequent allograft dysfunction. We show that $CD4^+CD57^+PD1^+$ T cells emerge in stable lung transplant recipients in the first year post-transplant, conferring heightened risks for CLAD and death or re-transplantation. $CD4^+CD57^+PD1^+$ T cells display features of senescence and secrete inflammatory cytokines. Cellular indexing by transcriptomes and epitopes (CITE-Seq) on BAL $CD4^+$ T cells revealed the existence of 2 oligoclonal $CD57^+$ subsets with putative cytotoxic and follicular helper functions. Finally, we observed that $CD4^+CD57^+PD1^+$ T cells are associated with lung allograft fibrosis in a mouse model and in human explanted CLAD lungs, where they localize near airway epithelium and B cells. Together, our findings reveal the existence of an inflammatory T cell population that predicts future lung allograft dysfunction and may represent a rational therapeutic target in lung transplant recipients.

Introduction

The study of allograft rejection has led to important advances in our understanding of cellular immunity[1]. Unfortunately, solid organ transplantation continues to be hampered by high rates of chronic rejection and graft failure despite the availability of potent immunosuppressive drugs. In lung transplantation (LT), which remains the only life-prolonging therapy for many cases of end-stage lung disease, median graft survival is only 6 years[2] due to chronic lung allograft dysfunction (CLAD). CLAD is the result of a progressive scarring process due to accumulated injuries resulting from alloreactivity and innate immune activation caused by donor brain death, ischemia-reperfusion injury, post-transplant infections, gastroesophageal reflux, and air pollution[3]. Both acute T cell-mediated rejection and antibody-mediated rejection are well-recognized CLAD risk factors[4,5].

LT recipients often grapple with episodes of acute lung allograft dysfunction (ALAD)[6]. We characterized ALAD as a marked decrement in lung function – quantified by a decline in the forced expiratory volume in one second (FEV_1) by 10% or more from its prior value. Despite exhaustive history, physical examination, and diagnostic testing including thoracic imaging and bronchoscopy, the cause of ALAD often is not definitively identified. Recurring ALAD events may be the result of rejection or uncontrolled alloimmunity that cannot be identified due to the poor diagnostic accuracy of transbronchial biopsies [7,8].

Bronchoalveolar lavage (BAL) is a technique in which saline instilled via a bronchoscope wedged in a pulmonary segmental airway is aspirated into a collection trap. BAL permits microbiologic and cytologic analysis of the distal lung compartments including the small airways and alveolar spaces. We have been studying cellular elements of the BAL using advanced multiparametric analytical approaches for the last several years[6,9-13]. Using single-cell RNA sequencing, we recently identified specific alveolar macrophage populations associated with ALAD episodes and CLAD[6], which may represent both a mechanistic link between inflammatory insults such as infection and rejection, as well as a potential target for therapeutic intervention.

Prior studies by several groups have examined specific BAL T cell populations in LT recipients. Early work examined the question of whether changes in the CD4:CD8 ratio

among BAL T cells might differentiate infection from rejection[14]. Later studies examined whether T cell activation[15], differentiation[16], regulatory T cells[17] and apoptosis[18] could distinguish CLAD, acute rejection and infection[19]. High variability between LT recipients meant that such distinctions were difficult[19] and not useful in an individual patient. Moreover, since acute rejection and infection and CLAD can all coexist, and there are large overlaps in the distributions of pre-specified BAL immune cell populations between these clinical entities, these hypothesis-directed analyses have not led to the identification of useful biomarkers or mechanistic insights.

Here, we used mass cytometry[20] – a high-dimensional technique in which the expression of up to 40 cell-associated proteins can be analyzed simultaneously, coupled with unbiased differential discovery approaches – to identify $CD4^+CD57^+PD1^+$ T cells as a predictor of incident ALAD and CLAD. Apart from their usefulness as a biomarker, our data implicate $CD4^+CD57^+PD1^+$ T cells in the mechanism of allograft loss. We find the cells in chronically rejected human and mouse lung allografts, show that they are clonally expanded, express transcripts associated with cytotoxic and helper functions, and they secrete inflammatory cytokines. Further, they are senescent, hypoproliferative, and resistant to cell death *in vitro.* Our observations therefore suggest the existence of a specific alloimmune pathway that can escape conventional immunosuppression that may represent a valuable therapeutic target.

Results

Identification of a T cell subset associated with lung allograft dysfunction

Early detection of alloimmune responses in the graft – *before* ALAD occurs – is likely to provide both important prognostic information as well as an opportunity for early intervention. In pursuit of a greater understanding of ALAD mechanisms, we prospectively collected and viably cryopreserved BAL cells from 50 Toronto Lung Transplant Program (TLTP) LT recipients presenting for surveillance bronchoscopy at 3 months post-transplant, and obtained two more follow up samples from each recipient to form a longitudinal cohort **(Figure 1A; Supp Fig 1)**. We performed mass cytometry[20] using a panel of 36 heavy metal-conjugated antibodies **(Supp Table 1)**. Conventional flow cytometric gating revealed considerable inter- and intra-patient heterogeneity in BAL cell composition (data not shown). Unsupervised multidimensional clustering using FlowSOM [21] demonstrated similar variation **(Figure 1B, C)**. In order to facilitate identification of cell populations associated with allograft dysfunction, we randomly divided the cohort into discovery and validation subsets (n=25 each; **Supp Table 2**). Longitudinal samples in the discovery group were then used to search for differences in the BAL cellular composition between stable patients and those experiencing ALAD within 30 days of each bronchoscopy. Initially we employed cluster identification, characterization and regression (CITRUS[22]) on all BAL T cells from all the time-points for all patients in the cohort. This analysis revealed that $CD4^+CD57^+PD1^+$ T cells were the top differentially represented cell population between patients with and without ALAD within 30 days of at least one bronchoscopy **(Figure 1D-F)**. CITRUS does not adequately account for the paired design of our cohort (multiple samples per patient), nor does it incorporate time as a factor in the analysis. We therefore also applied a generalized linear mixed model (GLMM) pipeline described for CyTOF analysis[23]. To facilitate this analysis, we used FlowSOM to identify 20 clusters of T cells **(Figure 1G)**. T cell subsets with greater representation in samples associated with ALAD compared to samples associated with stability were identified using this approach **(Figure 1H)**, revealing that the $CD4^+$ $CD57^+PD1^+$ T cell population – among several others – was significantly differentially represented in ALAD. Collectively, these data suggested that there is an association between $CD4^+CD57^+PD1^+$ T cells and incident ALAD.

$CD4^+CD57^+PD1^+$ T cells appear in the BAL prior to the onset of allograft dysfunction

Next, we assessed the relationship of BAL $CD4^+CD57^+PD1^+$ T cells to ALAD onset. We observed that while patients with stable lung allograft function had low frequencies of $CD57^+PD1^+$ cells in the BAL $CD4^+$ T cell compartment (**Figure 2A**), these cells typically accumulated in higher frequencies prior to the onset of ALAD **(Figure 2B)**. Receiver-operating characteristic (ROC) curve analysis showed that having ≥ 7.8% $CD57^+PD1^+$ cells in the BAL $CD4^+$ T cell compartment optimally discriminated concurrent ALAD from stable patients, with an area under the ROC curve of 0.76 **(Figure 2C)**. Using this criterion, 10 of 11 (91%) LT recipients with ALAD within 30 days of any of their bronchoscopies demonstrated ≥ 7.8% $CD57^+PD1^+$ in the $CD4^+$ T cell compartment of at least one of their BAL samples; in contrast, only 3 of 14 (21%) stable LT recipients had $CD57^+PD1^+$ cells exceeding this threshold **(Figure 2D)**. Moreover, having this biomarker conferred a reduced time-to-ALAD in univariable survival analysis **(Figure 2E)**. We then applied the 7.8% threshold to the validation subset (n=25) and observed a similar reduction in time-to-ALAD from first appearance of the cells in LT recipients with at least one BAL sample in which it was exceeded, compared to LT recipients who did not have any BAL samples in which the threshold was exceeded **(Figure 2F)**. Together, these data illustrated that in LT recipients developing subsequent allograft dysfunction, $CD57^+PD1^+$ cells frequently exceeded the 7.8% threshold in BAL samples obtained prior to ALAD and CLAD **(Supp Fig 2).**

Anti-human leukocyte antigen donor-specific antibodies (DSA) are an adverse prognostic factor in lung transplantation[24]. Patients with ≥7.8% $CD57^+PD1^+$ cells in the BAL $CD4^+$ T cell compartment were more likely to develop de novo DSA than those without **(Figure 2G)**. BAL $CD4^+CD57^+PD1^+$ T cells were not simply a surrogate for other conventional clinical and bronchoscopic parameters, since clinical symptoms, biopsy-proven vascular or airway rejection, BAL pathogens and antimicrobial treatments did not differ significantly between patients with and without ≥ 7.8% $CD57^+PD1^+$ cells in the BAL $CD4^+$ T cell compartment **(Supp Table 3)**. Similarly, although the number of events was small, having $CD57^+PD1^+$ cells above the 7.8% threshold was not clearly

109 associated with an immediate post-bronchoscopy augmentation of immunosuppression
110 or change in calcineurin inhibitor **(Supp Table 4)**. Taken together, these observations
111 indicate that BAL $CD4^+CD57^+PD1^+$ T cells may be a useful biomarker of incident lung
112 allograft dysfunction that adds significant diagnostic utility to conventional clinical
113 monitoring.

114 **$CD4^+CD57^+PD1^+$ T cells confer an increased risk for CLAD and death and are**
115 **present in chronically rejected human lung allografts**

116 To examine whether the presence of $CD4^+CD57^+PD1^+$ T cells in the BAL samples of LT
117 recipients increase the risk for CLAD, we followed all 50 individuals in our cohort for up
118 to 2000 days post-LT (median follow-up 1788 days). Using the appearance of ≥7.8%
119 $CD57^+PD1^+$ cells in the BAL $CD4^+$ T cell compartment or the last analyzed BAL as the
120 index event, we found that time to CLAD was significantly shorter in those patients whose
121 BAL samples exceeded the 7.8% threshold (log rank p=0.0071, **Supp Figure 3A**). We
122 then performed Cox proportional hazards analysis, excluding two patients who developed
123 CLAD prior to their final BAL samples (**Supp Fig 1**). Treating the appearance of ≥7.8%
124 $CD57^+PD1^+$ cells in the BAL $CD4^+$ T cell compartment as a time-dependent covariate,
125 Cox proportional hazards analysis revealed a hazard ratio (HR) of 3.61 (95% CI 1.55-
126 8.39) for time-to-CLAD. In this and other survival analyses, patients were followed until
127 31 December 2022 (median follow up time from transplantation: 2245 days). The
128 increased risk for CLAD associated with $CD4^+CD57^+PD1^+$ cells persisted in bivariable
129 models adjusted for age at transplant (HR 3.67, 95% CI 1.57-8.55), sex (HR 3.45, 95%
130 CI 1.47-8.07), and primary cytomegalovirus (CMV) mismatch (donor seropositive,
131 recipient seronegative; HR 4.02, 95% CI 1.70-9.52).

132 Similarly, a Cox proportional hazards model revealed that ≥7.8% $CD57^+PD1^+$ cells in the
133 BAL $CD4^+$ T cell compartment was associated with a HR of 4.82 (95% CI 1.8-13.1) for
134 time-to-death or retransplantation. The effect persisted in bivariable models adjusting for
135 age at transplant (HR 4.82, 85% CI 1.8-13.1), sex (HR 4.84, 1.8-13.2) and primary CMV
136 mismatch (HR 4.92, 95% CI 1.8-13.4). These time-to-CLAD and time-to-death or
137 retransplantation analyses are presented in **Supp Table 5**. We then examined time-to-
138 death or retransplantation in a survival analysis landmarked at 12 months post-transplant.

139 LT recipients with ≥ 7.8% $CD57^+PD1^+$ cells in the BAL $CD4^+$ T cell compartment had an
140 increased risk of death or retransplantation (p=0.00079, **Figure 3A**).

141 These observations suggested that $CD4^+CD57^+PD1^+$ T cells may lie on the mechanistic
142 pathway leading to lung allograft fibrosis. Therefore, we sought to identify them in CLAD
143 lung tissue obtained at the time of retransplantation[25] using imaging mass cytometry
144 (IMC[26]). CLAD and normal lung tissue sections were stained with a panel of 35 heavy
145 metal conjugated antibodies **(Supp Table 6)** and subjected to IMC. Unsupervised
146 clustering identified $CD4^+CD57^+PD1^+$ T cells as one of the cell populations present
147 (cluster 50 in **Figure 3B, Supp Fig 3B**), with more cells in CLAD compared to normal
148 tissue (**Figure 3C-D**). Image reconstruction and proximity analysis revealed that
149 $CD4^+CD57^+PD1^+$ T cells were frequently located adjacent to distinct B cell populations,
150 including trafficking B cells (CD20+CCR6+, Cluster 8) and plasma cells (IgM+CD138+,
151 cluster 30) and airways **(Figure 3E-F)**.

152 **$CD4^+CD57^+PD1^+$ T cells infiltrate mouse lung allografts and associate with the**
153 **severity of chronic rejection**

154 We have developed a minor alloantigen-mismatched mouse orthotopic lung transplant
155 model in which a minimal graft storage period prior to transplantation results in mild or
156 absent allograft fibrosis at 28 days post-transplant, while prolonged warm and cold
157 ischemic storage prior to transplantation leads to B cell- and alloimmune-dependent
158 fibrosis with features of human chronic lung allograft rejection[27] (**Figure 4A-B**). We asked
159 whether $CD4^+CD57^+PD\text{-}1^+$ T cells might be found within lung allografts in this model, and
160 whether their abundance correlated with the degree of allograft fibrosis. Allografts were
161 scored in blinded fashion using our published scoring system[28], which includes
162 assessment of the proportion of the allograft affected by interstitial inflammation and
163 fibrosis. As we have observed previously[27,28], pathology was variable, with some animals
164 exhibiting higher degrees of fibrosis and inflammation (**Fig 4C**). Flow cytometry performed
165 on single-cell suspensions of digested lung allograft tissue revealed that $CD57^+PD1^+$ T
166 cells were common among lung allograft $CD4^+$ T cells, but rare in normal lung tissue
167 (**Figure 4D**). It also showed that allografts with higher degrees of pathology – as
168 determined by the presence of both interstitial inflammation and parenchymal fibrosis –

169 had higher frequencies of CD57$^+$PD1$^+$ T cells compared to those with a low degree of
170 pathology (**Figure 4E-F**). Further, CD4$^+$CD57$^+$PD1$^+$ T cells were readily detectable in
171 allograft sections by immunofluorescence (**Figure 4G**). Together, these data support the
172 concept that CD4$^+$CD57$^+$PD1$^+$ T cells accumulate in rejecting lung allografts and correlate
173 with the severity of inflammation and fibrosis in mice.

174 **Identification of two transcriptionally distinct CD4$^+$CD57$^+$PD1$^+$ cell subsets using**
175 **CITE-Seq**

176 To characterize gene expression in CD4$^+$CD57$^+$PD1$^+$ T cells, we enriched CD3$^+$ T cells
177 from four ALAD BAL samples and performed cellular indexing by transcriptomes and
178 epitopes (CITE-Seq[29]) with 5' end sequencing. We applied a panel of oligonucleotide-
179 conjugated antibodies, including CD4, CD57 and PD1, to ALAD BAL samples containing
180 at least 7.8% CD57$^+$PD1$^+$ cells in the CD4$^+$ T cell compartment as determined by flow
181 cytometry. The conjugated oligonucleotides or antibody-derived tags (ADTs) identified in
182 CITE-Seq allowed confident linkage of transcriptomes with protein expression.

183 BAL CD4$^+$ T cells from patients with ALAD fell into 9 subclusters in multidimensional
184 space (**Figure 5A**). Based on CD57 and PD1 protein expression, CD4$^+$CD57$^+$PD1$^+$ T
185 cells assembled into two main areas, cluster 4 and the closely adjacent clusters 1 and 2
186 **(Figure 5A)**. We noted that CD27 gene and protein expression was enriched in cluster
187 4 compared to clusters 1 and 2 **(Figure 5B).** The CD27$^-$ population had a gene
188 expression profile similar to peripheral helper T (Tph) cells described in rheumatoid
189 arthritis[30]; differentially expressed genes in this population included CXCL13, TOX, IL-
190 21, CD40L, TIGIT, ICOS and TNFSRF18 **(Figure 5C)**. These cells are characterized by
191 the absence of the conventional follicular helper T cell markers CXCR5 and Bcl6, and
192 by expression of the chemokine CXCL13 [30,31]. Accumulating studies have shown that
193 Tph cells are involved in various acute and chronic inflammatory diseases [30,32]. Tph
194 cells can promote B cell differentiation into plasmablasts through interactions involving
195 IL-21 and SLAMF5 [30]. Therefore, the Tph-like features of CD27$^-$ CD4$^+$CD57$^+$PD1$^+$ T
196 cells, along with their proximity to B cells **(Figure 3E-F)**, their association with de novo
197 DSA **(Figure 2G)** suggest that they may provide B cell help.

198 The CD27$^+$ population expresses several cytotoxicity-related transcripts including
199 granzymes and NKG7[33] **(Figure 5C)**. They also express CXCR6, which has been
200 associated with tissue resident memory CD8$^+$ T cell localization to airways[34] and is in
201 keeping with our observation of CD4$^+$CD57$^+$PD1$^+$ T cells in proximity to airways **(Figure**
202 **3F)**.

203 We next examined TCR CDR3 sequences in the CITE-Seq data, which revealed that
204 CD57$^+$PD1$^+$CD27$^-$ cells are clonally expanded to a greater extent than CD57$^+$PD1$^+$CD27$^+$
205 and other BAL CD4$^+$ T cells **(Figure 5D)**. This suggested that they had recently
206 undergone antigen-driven expansion in the lung. Analysis of the top 20 expanded TCR
207 clonotypes did not infer any known antigen. However, the high similarity among the top
208 20 expanded TCRs may suggest that they are alloreactive **(Supp Figure 5).** Pseudotime
209 trajectory analysis revealed that CD57$^+$PD1$^+$CD27$^-$ cells and their CD27$^+$ counterparts
210 may share a common origin **(Figure 5E)**. Together, the TCR sequence data and
211 pseudotime analysis suggested that BAL CD4$^+$CD57$^+$PD1$^+$ T cells either differentiate into
212 Tph or cytotoxic effector cells. The former have undergone significant clonal expansion,
213 whereas the latter have a distinct TCR repertoire and less clonal expansion, suggesting
214 that they may be responding to different antigens in the lung microenvironment.

215 Finally, both CD27$^-$ and CD27$^+$ subsets demonstrated expression of previously defined
216 senescence and exhaustion transcripts including TIGIT, KLRG1, LAG3, HAVCR2/TIM-3
217 and EOMES which have been described in different acute and chronic inflammatory
218 conditions[35-37] . This observation is in keeping with reports that have described different
219 senescent CD57$^+$ and/or PD1$^+$ T cell populations in other disease states [38,39].

220 **Functional analysis of CD4$^+$CD57$^+$PD1$^+$ T cells reveals features of inflammation**
221 **and senescence**

222 Considering the potential distinct functional properties – Tph, cytotoxic, and senescent –
223 of CD4$^+$CD57$^+$PD1$^+$ T cells, we set out to characterize their functions *in vitro*. For this
224 purpose, CD4$^+$ T cells from BAL samples of 15 lung transplant recipients experiencing
225 ALAD were sorted to obtain CD4$^+$CD57$^+$PD1$^+$ T cells and their CD4$^+$CD57$^-$PD1$^-$
226 counterparts **(Figure 6A)**. Fluorescence-activated cell sorting data demonstrated that in
227 all cases, CD57$^+$PD1$^+$ cell frequency was ≥7.8% of BAL CD4$^+$ T cells **(Figure 6B)**. Based

228 on the hypothesis that $CD4^+CD57^+PD\text{-}1^+$ T cells may be senescent, we predicted that
229 sorted cells would exhibit decreased proliferation, enhanced cytokine secretion, and
230 resistance to TCR restimulation-induced cell death (RICD) when compared to $CD57^-PD1^-$
231 cells.

232 Supernatants from cells stimulated overnight were collected and subjected to a
233 multiplexed cytokine assay. This revealed that $CD4^+CD57^+PD1^+$ cells – compared to
234 $CD4^+CD57^-PD1^-$ cells sorted from the same BAL samples – expressed more IL-21, IL-4,
235 CXCL8 and granzyme A **(Figure 6C)**. In keeping with our CITE-Seq data, these findings
236 suggested that $CD4^+CD57^+PD1^+$ T cells may have Tph or cytotoxic properties – or both.
237 Stimulated $CD4^+CD57^+PD1^+$ T cells and their $CD57^-PD1^-$ counterparts were then tested
238 for proliferation, based on dilution of CFSE **(Figure 6D).** Proliferation data revealed that
239 $CD4^+CD57^+PD1^+$ T cells exhibited significantly less proliferation compared to $CD4^+CD57^-$
240 $PD1^-$ cells **(Figure 6E)**, in keeping with T cell senescence [38,39]. Finally, $CD4^+CD57^+PD1^+$
241 T cells were less susceptible to RICD compared to $CD4^+CD57^-PD1^-$ cells **(Figure 6F, G)**.
242 Together these data imply that $CD4^+CD57^+PD1^+$ T cells are senescent but pro-
243 inflammatory T cells that are resistant to antigen-induced death. These observations may
244 help to explain the emergence of ALAD and CLAD in lung transplant recipients despite
245 potent triple-drug immunosuppression, which would be predicted to be less effective
246 against these cells.

Discussion

247 In this study, we used a high dimensional mass cytometric discovery approach to
248 identify a T cell population in lung transplant recipient BAL that is associated with a
249 heightened risk for future allograft dysfunction, failure, and death. The risk conferred by
250 the appearance of $CD4^+CD57^+PD1^+$ T cells in the BAL remained elevated after bivariate
251 adjustments for age, sex, and donor and recipient CMV serostatus mismatch.

252 In keeping with previous work examining lung transplant recipient BAL, our samples
253 contained a diversity of leukocyte populations. The prior studies demonstrated
254 statistically significant relationships between BAL $CD8^+$ T cells, NK cells, eosinophils,
255 Tregs and outcomes in lung transplantation, but this has not led to meaningful
256 improvements in clinical care because wide overlaps in the frequency distributions of
257 these populations have meant that they lack discriminatory power in individual
258 patients[14,15,19,40-43]. In contrast, while $CD4^+CD57^+PD1^+$ T cells will require further
259 validation in larger studies, their prevalence among $CD4^+$ T cells discriminated patients
260 who remained stable from those about to undergo ALAD with high precision, in a
261 discovery cohort and confirmed in an independent validation cohort. Our observation
262 therefore represents a promising biomarker that may, in the future, permit the selection
263 of lung transplant recipients for targeted preventative interventions.

264 A review of clinical and laboratory variables present at the time of each bronchoscopy
265 did not reveal any clear association between the appearance of ≥ 7.8% $CD57^+PD1^+$ T
266 cells in the BAL $CD4^+$ T cell compartment and other indicators of lung allograft
267 inflammation or dysfunction. This observation likely reflects the relatively poor
268 performance of histopathologic and cytologic findings in the diagnosis of lung allograft
269 rejection. Indeed, interpretation of transbronchial biopsy histology is fraught, with high
270 rates of ungradable biopsies and substantial inter-observer disagreement among
271 pathologists[7,8]. It is therefore perhaps not surprising that bronchoscopies with high
272 frequencies of $CD4^+CD57^+PD1^+$ T cells showed no particular association with histologic
273 rejection. Likewise, we found that this T cell population is not a marker of lung allograft
274 infection, since there were no differences in pathogen isolation from the same BAL
275 samples. Our interpretation of these findings is that analysis of BAL $CD4^+CD57^+PD1^+$ T

276 cells may dramatically improve the utility of surveillance bronchoscopy after LT, which
277 will require further evaluation in larger prospective studies.

278 Beyond their value as a biomarker of future allograft dysfunction, several lines of
279 evidence support the notion that $CD4^+CD57^+PD1^+$ T cells are mechanistically relevant
280 to the pathogenesis of chronic lung allograft rejection and fibrosis. First, our CITE-Seq
281 data indicate that the majority of clonally expanded $CD4^+$ T cell populations in the BAL
282 of patients with ALAD were $CD57^+PD1^+$, which indicates that these cells have
283 undergone antigen-driven expansion in the lung. Further, in addition to their appearance
284 in BAL, we detected $CD4^+CD57^+PD1^+$ T cells in human explanted CLAD lung tissue
285 obtained at the time of re-transplantation. The cells were observed in proximity to B
286 cells and small airways; coupled with the finding that the transcriptome and secretome
287 of BAL $CD4^+CD57^+PD1^+$ T cells includes IL-21 and granzymes, this observation
288 suggests that they are likely participating in allograft injury and may subserve Tph
289 functions. In support of this assertion, in our ischemia-reperfusion injury-augmented
290 mouse model of human CLAD, we observed $CD4^+CD57^+PD1^+$ T cells in the lung
291 allografts of mice with marked fibrotic pathology. In contrast, allografts with milder
292 fibrosis did not contain many $CD4^+CD57^+PD1^+$ T cells. Interestingly, we have previously
293 shown that fibrosis in this model is B cell dependent[27], and so in future work it will be
294 important to consider the possible existence of a $CD4^+CD57^+PD1^+$ T cell-B cell axis that
295 drives chronic lung allograft rejection in mice and humans.

296 PD-1 expression by $CD8^+$ T cells in tumor microenvironments is associated with cancer
297 progression, and generally reflects a state of exhaustion in which effector functions are
298 deactivated. BAL $CD4^+CD57^+PD1^+$ T cells also expressed several additional molecules
299 that have been associated with exhaustion, including TIM-3, LAG3 and CTLA-4. While
300 analysis of the cells *ex vivo* revealed that they were both hypoproliferative and resistant
301 to T cell RICD, their production of inflammatory cytokines – which is not a feature of
302 exhaustion – suggests that they are senescent rather than exhausted. Of note,
303 senescent $CD4^+$ and $CD8^+$ T cells in humans were described as having the phenotype
304 $CD45RA^+KLRG1^+CD57^+CD28^-CD27^-$ [44,45] Animal and human data indicate that
305 senescent T cells participate in other chronic inflammatory, degenerative and metabolic
306 disorders[39].

307 Lung transplant recipients typically receive immunosuppressive drugs – calcineurin
308 inhibitors, corticosteroids, and antimetabolites – in much higher doses than other solid
309 organ transplant recipients, and yet also have the highest rates of acute and chronic
310 allograft rejection. With respect to T cells, these drugs act by inhibiting cell proliferation.
311 In this context, we speculate that $CD4^{+}CD57^{+}PD1^{+}$ T cells, which exhibit reduced
312 proliferation, escape this inhibition and can continue to produce cytokines. Further work
313 will be required to understand how these cells arise within the lung allograft, and
314 whether specific targeting of these cells may have a therapeutic benefit.

Methods

315 **Study design and BAL collection**

316 The samples analyzed in this study were collected with informed consent for research
317 use and were approved by University Health Network Research Ethics Board (15-9531).
318 BAL cells from 50 TLTP lung transplant recipients presenting for surveillance
319 bronchoscopy at 3 months post-transplant were obtained according to a standard
320 protocol [46]. In addition, for each LT recipient, two further samples were obtained from
321 each recipient to form a longitudinal cohort **(Supp Fig 1)**. Cells were centrifuged at 400g
322 for 5 min and resuspended in 1 ml of 10% dimethyl sulfoxide/90% FBS for viably
323 cryopreservation. Cryovials were placed in Mr. Frosty containers at -80°C for 24 h, then
324 stored in liquid nitrogen until thawing for processing and mass cytometry. BAL cells from
325 a further 14 LT recipients with acute lung allograft dysfunction (ALAD, defined as a
326 decrease in the forced expiratory volume in one second [FEV1] by 10% or more from
327 the baseline FEV1 measurements) were used for sorting fresh $CD4^{+}CD57^{+}PD1^{+}$ T cells
328 and their $CD57^{-}PD1^{-}$ counterparts for functional analyses.

329

330 **Mass cytometry**

331 Metal-conjugated antibodies were either purchased preconjugated from Fluidigm or
332 purchased purified from BioLegend, Thermo Fisher Scientific or BD Biosciences and
333 subsequently conjugated to metals using Maxpar Antibody Labeling Kits (Fluidigm)
334 according to the manufacturer's instructions **(Supp Table 1)**. Cryopreserved samples
335 were recovered and divided into stimulated (with PMA 50ng/mL and ionomycin
336 500ng/mL) and unstimulated conditions to allow analysis of cytokine secretion
337 expression and surface markers. Cells were incubated with a cocktail of antibodies
338 against cell surface molecules for 30 min at room temperature. After treatment with
339 intracellular fixation and permeabilization buffers (BD Biosciences), cells were incubated
340 with metal-conjugated antibodies against intracellular proteins. Cells were then washed
341 and stained with Intercalator-Ir (Fluidigm) diluted in PBS containing 1.6%
342 paraformaldehyde and stored at 4 °C until next-day acquisition. To address technical
343 variations between mass cytometry runs, a control healthy volunteer PBMC sample was
344 aliquoted, recovered and stained and analyzed alongside the BAL samples.

345 **Mass cytometry data analysis**

346 Mass cytometry data were initially analyzed with manual gating to exclude debris, dead
347 cells and doublets and to select CD45+ cells using Cytobank software (Beckman
348 Coulter). We then used the FlowSOM and viSNE algorithms (5,000 iterations,
349 perplexity = 100) for visualization of high-dimensional data [21,47]. Subsequently, we
350 applied cluster identification, characterization, and regression (CITRUS) [22] on the CD3+
351 population from the discovery cohort (n=25, **Supp Table 2**) to identify cell subsets
352 associated with ALAD within 30 days of the sample. CITRUS was run at least 5 times
353 with "equal number" of cells per sample, looking for "abundance" as cluster
354 characterization, with a 1% false discovery rate. To incorporate the time-course design
355 of our study, we implemented a generalized linear mixed model analysis-adapted R
356 pipeline as described by Nowicka and colleagues [23]. In this approach, different
357 timepoints for each LT recipient were defined as a variable to allow intra-subject pairing.
358 Finally, we used manual gating to confirm the results of CITRUS and generalized linear
359 mixed model analysis.

360

361 **Imaging Mass Cytometry**

362 Lung tissue samples were obtained during retransplantation procedures from 8 patients
363 who were undergoing a second Lung Transplantation due to end-stage CLAD. A single
364 biopsy was obtained from the upper lobe of each patient presenting with CLAD. The
365 harvested lung tissue was initially inflated and immersed in a 10% formalin solution for
366 24 hours. Subsequently, it underwent immersion in a 70% ethanol solution for an
367 additional 24-hour period before being embedded in paraffin. Sections of the paraffin-
368 embedded lung tissue, with a thickness of 4µm, were prepared and affixed to slides for
369 further analysis. For every specimen, we meticulously identified three distinct 1x1mm
370 Regions of Interest (ROIs) situated around individual airways. In addition to the CLAD
371 patient samples, we included control samples in our study. Four lung biopsies were
372 procured: two from patients undergoing lobectomy procedures for suspected cancer
373 and two from surplus donor lung tissue collected at the conclusion of the cold ischemic
374 phase during lung transplantation. To facilitate our analysis, sections of the lung tissue
375 were subjected to staining using a panel of 35 heavy-metal-tagged antibodies

376 **(Supplementary Table 6)**. Subsequently, the three ROIs chosen for each specimen
377 were subjected to ablation using the Hyperion Imaging System developed by Fluidigm.
378 The ablation process employed a laser frequency of 200Hz, with laser power settings
379 ranging from 3.5 to 4.5. The ablation procedure generated files in both .txt and .mcd
380 formats, which were subsequently subjected to thorough analysis using the HistoCAT
381 software platform[48].
382
383 **Animal model**
384 Orthotopic lung transplantation was performed using C57BL/10 donors and C57BL/6
385 recipients under different graft preservation conditions as described previously [27].
386 Briefly, harvested lungs were stored either under minimal (60 minutes at 4ºC followed
387 by 15 min of warm anastomotic time) or prolonged (6h at 4ºC, 45 min at 37ºC, followed
388 by 15 min of warm anastomotic time) storage prior to reperfusion. Orthotopic lung
389 transplant recipients were sacrificed 28 days after LT for histological analysis and
390 cellular phenotyping. Grafts were flushed with saline and digested with collagenase A
391 and DNase I in a gentleMACS tissue dissociator (Miltenyi Biotec). Cells were stained
392 with cocktails of fluorochrome-conjugated monoclonal antibodies including AF647-
393 conjugated anti-mouse CD57 (polyclonal; Bioss) and AF488-conjugated anti-mouse
394 PD1 (polyclonal; Bioss). Flow cytometry data were analyzed using FlowJo (v10, FlowJo
395 LLC) and correlated with histological grading. We graded peribronchial fibrosis and
396 parenchymal fibrosis in a blinded fashion according to a published scoring system[28].
397 Immunofluorescent staining of sections of formalin-fixed and paraffin-embedded lung
398 tissue was conducted by antigen retrieval using 1x pH 9 Tris/EDTA buffer before
399 staining with unconjugated anti-mouse CD4. This was followed by a secondary antibody
400 cocktail including Alexa Fluor 555 anti-rabbit IgG (A-31572, Invitrogen) as well as
401 AF647-conjugated anti-mouse CD57 (polyclonal; Bioss) and AF488-conjugated anti-
402 mouse PD1 (polyclonal; Bioss). Nuclei were stained with DAPI and
403 immunofluorescence images were acquired using a Zeiss AxioObserver.
404
405 **CITE-seq sample processing and acquisition**

406 We identified four LT recipients scheduled for bronchoscopy with ALAD (FEV_1 decrease
407 by ≥10% from the prior value). Fresh BAL cells were collected by centrifugation at 400g
408 for 5 minutes. T cells were obtained using a $CD3^+$ T cell enrichment kit (EasySep™
409 Human T Cell enrichment, Stemcell Technologies) according to the manufacturer's
410 instructions. Enriched T cells were resuspended at $1x10^6$ cells/mL in PBS + 0.05% BSA.
411 50 µL of the cell suspension were stained with BV711 conjugated anti-human CD4,
412 APC conjugated anti-human PD1 and PE-Cy7 anti-human CD57 and analyzed by flow
413 cytometry to confirm ≥ 7.8% $CD57^+PD1^+$ cells in the BAL $CD4^+$ T cell compartment. If
414 confirmed, the remaining cells were used for CITE-seq. Briefly, $1x10^6$ cells were
415 resuspended in 45 µL PBS + 0.05% BSA before adding 5 µL of Fc blocking reagent and
416 incubated for 10 minutes at 4°C. TotalSeq™-C antibody cocktails were prepared during
417 the incubation by adding pre-determined concentrations of each antibody **(Supp Table**
418 **6)**. The resulting cocktail was then added to cells and incubated for 30 minutes at 4°C.
419 After incubation, the cell pellets were resuspended in 1mL PBS + 0.05% BSA and
420 centrifuged for 5 minutes at 400 x g. After a total of 3 washes, the final cell density was
421 adjusted to 1000-1200 cells/µL and subjected to the 10X Genomics Chromium 5'
422 Immune Profiling v2.0 protocol for library preparation. A total of 2×10^4 cells from each
423 sample were loaded onto a 10X single cell G chip. After droplet generation, samples
424 were transferred to a pre-chilled 96 well plate (Eppendorf), heat sealed and incubated
425 overnight in a Veriti 96-well thermocycler (Thermo Fisher). The next day, sample cDNA
426 was recovered using Recovery Agent (10X Genomics) and subsequently cleaned up
427 using Silane DynaBeads (Thermo Fisher) mix as outlined by the user guide 5' Immune
428 Profiling v2.0. Purified cDNA was amplified for 11 cycles before being cleaned up using
429 SPRIselect beads (Beckman Coulter). Samples were diluted 9:1 (elution buffer
430 (Qiagen):cDNA) and run on a Bioanalyzer (Agilent Technologies) to determine cDNA
431 concentration. The library was then sequenced using an Illumina Novaseq 6000
432 sequencer using the following parameters Read 1: 28b, index 1: 10bp, Index 2: 10bp,
433 Read 2: 90bp.
434
435
436 **CITE-seq analysis**

437 The sequencing output was first demultiplexed and converted into FASTQ files using
438 Cell Ranger [49]. Reads were aligned to the human reference genome (grch38), and
439 count UMIs in the mRNA libraries, and CITE-seq-Count to count UMIs in the antibody-
440 derived tag (ADT) libraries. The matrix, barcodes, and gene information from Cell
441 Ranger were then used to create gene-cell matrices and a Seurat object [50]. For each
442 Seurat object, cells with poor quality were excluded based on the following quality
443 control metrics: unique gene counts over 5000 or below 200, UMI counts over 30,000,
444 and mitochondrial gene expression higher than 10%. Each sample was scaled and
445 normalized using Seurat's "SCTransform" function followed by adding the protein
446 expression levels to the Seurat object and normalization and scaling for ADT assay.
447 Next, $CD4^+$ T cells were subsetted based on high CD4 and low CD8 protein expression
448 (ADT-CD8 < 12 & ADT-CD4 > 12). Seurat objects of CD4+ cells from all four BAL
449 samples were merged into a single Seurat object. The SCTransform method was used
450 for normalization, scaling, and integration which corrects for unwanted sources of
451 variation and enhances the signal of genuine biological differences between cells[51].
452 Then, dimensionality reduction was applied to the integrated Seurat object, allowing
453 visualization and interpretation of the high-dimensional scRNAseq data. This was
454 followed by unsupervised clustering (resolution = 0.5) which led to the identification of
455 10 clusters. Then cells with higher expression of protein level of CD57 and PD1 were
456 highlighted on tSNE plot.
457 RNA velocity estimates the future state of individual cells by calculating the ratio of
458 unspliced to spliced mRNA for each gene. The spliced and unspliced counts from the
459 scRNAseq data were utilized to calculate RNA velocity using the velocyto package in
460 Python[52]. Splicing information extracted from velocyto was then added to all the
461 selected cells in the $CD4^+$ Seurat object. Subsequently, $CD4^+$ T cells underwent
462 pseudotime trajectory analysis using the scVelo pipeline[53]. This analysis inferred the
463 trajectory and the chronological sequence of cell states, highlighting the differentiation
464 paths taken by cells. The pseudotime values were visualized on the tSNE plots,
465 providing insights into the dynamic processes and cellular transitions at play.

466 **Fluorescence-activated cell sorting**

467 BAL cells collected from 15 ALAD samples and stained with fluorophore-tagged surface
468 antibodies for 30 min at room temperature. The following antibodies were used to stain
469 the cells: BV711-conjugated anti-human CD4 (BioLegend); APC-conjugated anti-human
470 PD1 (BioLegend); PE/Cy7-conjugated anti-human CD57, in addition to biotinylated
471 CD163, CD14, CD8, and CD56 (all from BioLegend). Cells washed with 500 µL of 1%
472 FBS in PBS and incubated with streptavidin-AF488 (1:200, BioLegend) for 20 minutes,
473 before washing and staining with propidium iodide to identify dead cells. Stained cells
474 were subjected to FACS sorting using a Sony SH800 instrument. After exclusion of PI-
475 positive cells and putative doublets based on forward and side scatter analysis, cells in
476 the dump channel (AF488) were eliminated. The remaining cells were gated to select
477 $CD4^+$ T cells and sorted for $CD57^+PD1^+$ and $CD57^-PD1^-$ cells.
478
479 **Cell culture, multiplex protein analysis, and *in vitro* assays**
480 Sorted cells were labeled with 1µM CFSE in serum free PBS prior to wash and culture
481 with plate bound anti-CD3 (5µM) and soluble anti-CD28 (1µM) antibodies in DMEM
482 medium containing 5.55 mM D-glucose, 4 mM L-glutamine, and 1 mM sodium pyruvate,
483 supplemented with 10% FBS, 50 U/ml penicillin, and 50 mg/ml streptomycin and 500
484 U/ml human recombinant IL-2 (Proleukin, Chiron). After 18 hours, 100µL supernatant
485 was replaced with fresh media. The collected supernatant was stored at -80°C for later
486 multiplex analysis. Supernatants were thawed and subjected to a custom multiplex bead
487 kit (R&D Systems) to assess the levels of released analytes including IL-21, IL-4,
488 CXCL8, and granzyme A. Samples were prepared in a 1:1 dilution with assay buffer, as
489 suggested by the manufacturer. Diluted samples and standards were run in duplicate.
490 Biomarker concentrations were obtained using a Bio-Plex MAGPIX Multiplex Reader
491 (Bio-Rad). All samples and standards were run in duplicate according to manufacturers'
492 protocols.
493
494 After 5 days, CFSE dilution in the sorted cells – a measure of T cell proliferation – was
495 determined by flow cytometry. Finally, a restimulation-induced cell death assay[54] was
496 used to assess whether $CD57^+PD1^+$ cells are less susceptible to this mode of cell death
497 than their $CD57^-PD1^-$ counterparts. $CD57^+PD1^+$ and $CD57^-PD1^-$ cells were stimulated in

498 culture for 7 days before washing, and were then restimulated with anti-CD3 mAb
499 (OKT3, 100 ng/ml final) for 24 hours. Cells were then harvested and stained with
500 Annexin V and propidium iodide for evaluation of apoptotic cell death.

501 **Statistics**

502 All statistical tests were two-sided unless stated otherwise. The Wilcoxon rank-sum test
503 was used to assess statistical differences between two groups. When assessing >2
504 groups simultaneously, the nonparametric Kruskal–Wallis test was used. A Fisher's
505 exact test was applied to assess statistical differences between two categorical
506 variables. Receiver Operating Characteristic (ROC) curves were used to assess
507 classification accuracy, which was quantified by Area Under the Curve (AUC). Kaplan–
508 Meier plots and two-sided log-rank tests were used to compare survival probabilities
509 between groups. Cox Proportional Hazards (PH) regression models were used to adjust
510 for potential confounders for time-to-CLAD or time-to-death/retransplantation analysis.
511 and Cox regression analyses were used to assess covariates with respect to time-to-
512 allograft dysfunction. All statistical analyses were performed using R v.3.5.1+ or Prism
513 8+ (GraphPad Software).

Figure legends

514 **Figure 1. Identification of a bronchoalveolar lavage (BAL) CD4$^+$ T cell population**
515 **associated with lung allograft dysfunction. A.** Study schematic. Fifty consecutive
516 patients presenting for bronchoscopy at 3 months post-transplant were enrolled. For
517 each enrolled patient, BAL cells at three time points (3mo, 6mo, 9mo or next available)
518 were collected. BAL cells were cryopreserved and subjected to mass cytometry (see
519 supplementary table 1); all samples from each patient were analyzed in the same mass
520 cytometry experiment. **B.** t-distributed stochastic neighbour embedding (tSNE) plots of
521 BAL CD45$^+$ cells falling into 20 clusters (highlighted in different colours) identified by
522 FlowSOM. **C.** tSNE plots highlighted by expression of 4 different lineage markers; CD3
523 (top left), CD11c (top right), CD56 (bottom left), CD19 (bottom right). **D.** CITRUS
524 (cluster identification, characterization, and regression) analysis of all BALs from n=25
525 discovery group patients showing cell populations differentiating patients developing
526 allograft dysfunction within 30 days from those whose allograft function remained stable.
527 Red circle indicates the statistically significantly differentially represented population. **E.**
528 Mass cytometry histograms of the top differentially represented population, which
529 expresses CD4, CD57, CD3 and PD1. **F.** Box-and-whisker plot showing the abundance
530 of CITRUS cluster 1076 – representing CD4$^+$CD57$^+$PD-1$^+$ T cells – which exhibited a
531 significant difference between ALAD and stable samples. **G.** t-SNE plot based on
532 arcsinh-transformed marker expression in 500 randomly selected cells per sample from
533 the discovery set (n=25, all 3 time points shown). Cells are coloured according to the 20
534 cell populations obtained with FlowSOM after the metaclustering step with
535 ConsensusClusterPlus. **H.** Differential analysis heatmap of arcsine-square-root
536 transformed cell frequencies that were subsequently normalized per cluster (rows, 20
537 clusters identified in the panel E). Statistically significant clusters are highlighted with
538 green and showing their p-values. **I.** Marker expression of clusters revealed that cluster
539 14 is significantly differentially represented between ALAD and stable patients
540 (highlighted with red rectangle), with a similar protein expression signature
541 (CD4$^+$CD57$^+$PD1$^+$) as identified by CITRUS.

542 **Figure 2. Relationship of BAL CD4$^+$CD57$^+$PD1$^+$ T cells with incident allograft**
543 **dysfunction.** Representative examples of forced expiratory volume in one second

544 (FEV1) over time in weeks post-transplant for stable (**A**) and ALAD (**B**) lung transplant
545 recipients in the discovery cohort. Weeks during which bronchoscopy was performed
546 are highlighted in yellow; scatterplots showing expression of CD57 and PD1 in the $CD4^+$
547 T cell compartment of the BAL are shown for each time point. Green line indicates 80%
548 of best post-transplant baseline, below which CLAD may be diagnosed. **C.** Receiver-
549 operator characteristic (ROC) curve analysis of the performance characteristics of
550 $CD57^+PD1^+$ cells as a proportion of the BAL $CD4^+$ compartment for diagnoses of
551 subsequent ALAD. The area under the curve (AUC) = 0.76. The percentage of
552 $CD57^+PD1^+$ T cells providing optimal discrimination of ALAD and stable patients (7.8%)
553 is circled in red. **D.** The highest proportion of $CD57^+PD1^+$ T cells observed in all BAL
554 samples from each patient (discovery cohort, n=25) is shown, divided by the presence
555 or absence of ALAD within 30 days. Mann-Whitney test p=0.0018. Dotted line shows
556 the 7.8% threshold identified in ROC curve in C. **E.** Time to lung allograft dysfunction
557 from the emergence of $CD57^+PD1^+$ cells $\geq$ 7.8% of $CD4^+$ T cells in the BAL (red line), or
558 from the final BAL analyzed (blue line) in the discovery cohort (n=25). Log rank test $p <$
559 0.0001. **F.** Time to lung allograft dysfunction from the emergence of $CD57^+PD1^+$ cells $\geq$
560 7.8% of $CD4^+$ T cells in the BAL (red line), or from the final BAL analyzed (blue line) in
561 the validation cohort (n=25). Log rank test $p < 0.02$. G. Of 28 patients who developed de
562 novo DSA, 19 (67.9%) had $CD57^+PD1^+$ cells $\geq$ 7.8% of $CD4^+$ T cells in at least one BAL
563 sample; only 9 of 23 (39.1%) patients who did not develop de novo DSA had
564 $CD57^+PD1^+$ cells $\geq$ 7.8% of $CD4^+$ T cells in at least on BAL sample. Chi square test p =
565 0.0402.

566 **Figure 3. $CD4^+CD57^+PD1^+$ T cells are associated with an increased risk of death or**
567 **re-transplantation and are found in CLAD lung tissue. A.** Kaplan-Meier curves
568 showing time to death or re-transplantation from 12 months post-transplant. Log-rank
569 test p = 0.00079. **B.** Selected heatmap of protein expression for selected clusters and
570 markers to highlight protein profile of cluster 50. **C.** Imaging mass cytometry of normal
571 donor lung tissue (left) and CLAD lung tissue obtained at the time of retransplantation
572 (right). E-cadherin$^+$ epithelial cells (green pseudocolour), red $CD3^+$ T cells (red
573 pseudocolour), $CD4^+$ cells (blue pseudocolour), and $CD4^+CD57^+PD1^+$ T cells (cluster
574 50, pale blue pseudocolour) are shown. **D.** $CD4^+CD57^+PD1^+$ T cells are more numerous

575 in CLAD lung tissue. Data from 3 regions of interest (ROIs) from each of n=8 CLAD, and
576 n=4 normal lungs are shown. **E.** In CLAD lung tissue, $CD4^+CD57^+PD1^+$ T cells (cluster
577 50, white) are found in association with airways (green pseudocolour E-cadherin$^+$ cells)
578 and with two distinct B cell populations (cluster 8, pale blue pseudocolour and cluster
579 30, purple pseudocolour). **F.** Cell-cell interaction heatmap shows association of
580 $CD4^+CD57^+PD1^+$ T cells (cluster 50) with epithelial cells (cluster 27) and B cells
581 (clusters 8 and 30). G. Liquid phase mass cytometry performed on single cell
582 suspensions obtained from CLAD lung tissue show variable presence of
583 $CD4^+CD57^+PD1^+$ T cells.

584 **Figure 4. $CD4^+CD57^+PD1^+$ T cells are associated with fibrosis in a mouse model of**
585 **chronic lung allograft rejection. A.** C57BL/10 (B10) donor lungs were subjected to
586 either prolonged (6h cold ischemic time (CIT) at 4°C followed by 1h warm ischemic time
587 (WIT) at 37°C) or minimal (60min CIT followed by 15min WIT) storage prior to orthotopic
588 left lung transplantation into minor alloantigen-mismatched C57BL/6 (B6) recipients. **B.**
589 After 28 days, paraffin-embedded sections of lung tissue were subjected to Masson
590 trichrome staining (200x magnification). **C.** Grafts were scored using a published
591 scoring system[28] that quantifies the percentage of the graft affected by interstitial
592 inflammation and parenchymal fibrosis. Grafts with high-grade pathology (High Path)
593 are represented as triangles, and those with minimal pathology (Low Path) are
594 represented as circles. **D.** Single-cell suspensions of naïve B6 lungs (No OLT) and lung
595 allografts obtained at 28 days post-transplantation were subjected to flow cytometry.
596 Analyses are gated on $CD4^+$ T cells. Percentages of cells in the $CD57^+PD\text{-}1^+$ gate are
597 shown in the representative plots. **E.** Percentage of $CD4^+$ T cells expressing CD57 and
598 PD-1 is shown for naïve B6 lungs (No OLT, squares), Low Path grafts (circles) and High
599 Path grafts (triangles). Student's t test, p=0.0005. **F.** Percentage of $CD4^+$ T cells
600 expressing CD57 and PD-1 is shown for Low Path grafts (circles) and High Path grafts
601 (triangles). Student's t test, p=0.0205. **G.** Immunofluorescence of prolonged storage,
602 High Path lung allograft showing PD1 (green), CD57 (red), CD4 (yellow) and DAPI
603 (blue) and merged image.

604 **Figure 5. Identification of distinct CD27$^+$ and CD27$^-$ subsets of CD4$^+$CD57$^+$PD1$^+$ T**
605 **cells.** Sequencing by CITE-Seq was performed on 4 BAL samples from patients with
606 ALAD. **A.** After downsampling and integration, BAL CD4$^+$ T cells (CD3$^+$CD4$^+$CD8$^-$
607 identified by antibody-derived oligonucleotide tag, adt) were displayed on a tSNE plot
608 revealing 10 distinct cell clusters (left tSNE plot). Feature plot showing CD57 adt and
609 PD1 adt labeling in CD4$^+$ cells as indicated by blue dots inside. Three distinct clusters
610 with detectable CD57 and PD1 protein expression are identified (1, 2, 4); however,
611 clusters 1 and 2 have combined as they have similar gene profile. **B.** tSNE plot
612 demonstrating CD27 expression in in RNA level (left) and protein level (adt, right). **C.**
613 Dot plot of the selected top differentially expressed genes in BAL CD4$^+$ T cells showing
614 the differences between CD27+ and CD27- associated gene profile. CD27- cells
615 contains LAG3$^+$ CXCL13$^+$ TNFRSF18$^+$ population suggesting putative peripheral helper
616 function while CD27$^+$ cells expressing GZMK$^+$ NKG7$^+$ EOMES$^+$ cells implying putative
617 cytotoxic CD4$^+$ T cells. **D.** tSNE plot highlighted by size of TCR expansion where yellow
618 is large TCR expansion and purple is single TCR. Selected tSNE with red dotted circle
619 shows highest frequency of expanded TCR in CD4+ cells. **E.** tSNE plot highlighted by
620 velocity trajectory shown by arrows. Same high frequency of TCR mentioned in D, was
621 identified red dotted circle implying cells from cluster 1, 2, and 4 originated from the
622 same cells.

623 **Figure 6. Functional properties of CD4$^+$CD57$^+$PD1$^+$ T cells. A.** CD4$^+$CD57$^+$PD1$^+$ T
624 cells can be identified by conventional flow cytometry. BAL cells were stained with CD4,
625 CD57 and PD1 antibodies and CD57$^+$PD1$^+$ cells were identified within the CD4$^+$
626 population, allowing quantification and cell sorting. **B**. Percentage of CD57$^+$PD1$^+$ cells
627 within the CD4$^+$ gate is shown for n=14 patients with ALAD. **C.** Sorted CD57$^+$PD1$^+$ and
628 CD57$^-$PD1$^-$ CD4$^+$ T cells from ALAD BAL samples were stimulated *in vitro* with anti-
629 CD3/anti-CD28 antibodies overnight. Culture supernatants were subjected to
630 multiplexed cytokine quantification. IL-21 (p=0.031), IL-4 (p=0.062), CXCL8 (IL-8,
631 p=0.031) and GZMA (p=0.062) were generally secreted in greater concentrations by
632 CD57$^+$PD1$^+$ T cells than their CD57$^-$PD1$^-$ counterparts, Wilcoxon matched-pairs signed
633 rank test. **D.** Example of sorted CD57$^+$PD1$^+$ (blue) and CD57$^-$PD1$^-$ CD4$^+$ (pink) T cells
634 from ALAD BAL were examined for proliferation by dilution of CFSE. CD57$^-$PD1$^-$ CD4$^+$

635 (pink) demonstrated potential to respond to CD3/CD28 stimulation by proliferation as
636 shown by several CFSE dilution picks. However, $CD57^+PD1^+$ cells did not proliferate
637 upon CD3/CD28 stimulation. **E.** Percentage of proliferation of $CD57^+PD1^+$ are
638 significantly lower compared to their $CD57^-PD1^-$ counterparts. Linked $CD57^+PD1^+$ and
639 $CD57^-PD1^-$ cells are sorted from same LT recipient. **F.** Example of sorted $CD57^+PD1^+$
640 and $CD57^-PD1^-$ counterpart T cells subjected to RICD assay demonstrated apoptosis in
641 response to CD3 restimulation in $CD57^-PD1^-$ while $CD57^+PD1^+$ are irresponsive. **G.**
642 Percentage of Annexin V as a marker apoptosis are significantly lower in $CD57^+PD1^+$
643 compared to their $CD57^-PD1^-$ counterparts. Linked $CD57^+PD1^+$ and $CD57^-PD1^-$ cells
644 are sorted from same LT recipient.
645
646 **<u>Supplementary figure legends</u>**
647
648 **Supp Fig 1. Study flow diagram for the BAL CyTOF cohort**.
649
650 **Supp Fig 2. Animated association between lung allograft dysfunction and**
651 **appearance of CD57+PD1+ T cells in individuals**. 50 LT recipient in CyTOF cohort
652 divided into two groups, discovery (1-25) and validation (26-50). For each individual LT
653 recipient, different events have been demonstrated. Events are included of appearance
654 $CD57^+PD1^+$ T cells (as blue cross), ALAD as blue triangle and CLAD as red triangle.
655 Orange line indicates time post-transplant with no exact timing relevance.
656
657 **Supp Fig 3. $CD4^+CD57^+PD1^+$ T cells are associated with an increased risk of CLAD**
658 **and are found in CLAD lung tissue. A.** Kaplan-Meier curves showing time to CLAD**.**
659 **B.** Imaging mass cytometry heatmap of 50 clusters (y axis) and their marker expression
660 in x axis.
661
662 **Supp Fig 4. Identification of distinct $CD27^+$ and $CD27^-$ subsets of $CD4^+CD57^+PD1^+$**
663 **T cells.** Sequencing by cellular indexing of transcriptomes and epitopes (CITE-Seq)
664 was performed on 4 BAL samples from patients with ALAD. **A.** After downsampling and
665 integration, BAL $CD4^+$ T cells ($CD3^+CD4^+CD8^-$ identified by antibody-derived

666 oligonucleotide tag, adt) were displayed on a tSNE plot revealing 10 distinct cell
667 clusters. Feature plot showing CD57 adt labeling in CD4+ cells as indicated by lavender
668 dots inside red circles. Three distinct clusters with detectable CD57 protein expression
669 are identified (1, 2, 4). **B.** Heat map of the top differentially expressed genes in BAL
670 $CD4^+$ T cells, with clusters identified in B highlighted in red boxes. Cluster 1 contains a
671 $CD27^-$ $LAG3^+$ $CXCL13^+$ $TNFRSF18^+$ population (putative follicular helper function).
672 Cluster 2 contains CD27-GZMA+CXCR6+CCL5+ cells (putative mucosa-associated
673 invariant T cells). Cluster 4 contains $CD27^+GZMK^+NKG7^+EOMES^+$ cells (putative
674 cytotoxic CD4+ T cells). **C.** Feature plot of selected genes related to high association
675 with Cluster 1, 2, and 4.
676
677 **Supp Fig 5. TCR analysis indicates high similarities between Clusters 1 and 2. A.**
678 Quantitative clonal expansion of TCRseq data suggested highest expansion from
679 cluster 2 (129 large clonal expansion). **B.** Top 20 expanded clones for each clusters
680 suggested high similarities between expanded clones of Cluster 1 and 2 while there is
681 limited similarities among those clones and top 20 clones of cluster 4.
682
683
684 **<u>Supplementary table legends</u>**
685
686 **Supp Table 1. Antibody panel for CyTOF.** Highlighted channels are intracellular
687 markers.
688
689 **Supp Table 2. Clinical characteristics of participants.** Patients were randomized into
690 a discovery group (n=25) and a validation group (n=25).
691
692 **Supp Table 3. Clinical and bronchoscopic parameters associated with ≥ 7.8%**
693 **$CD57^+PD1^+$ T cells in the BAL $CD4^+$ T cell compartment.** Fisher's exact tests were
694 performed. 1Missing samples excluded. 2Comparison of normal to abnormal cytology.
695 3Comparison of A0/AX with A1 or greater. 4Testing not done (n.d.) due to rarity of small
696 airway inflammation in the cohort. 5Comparison of any antimicrobial therapy pre- or
697 post-bronchoscopy vs. none. 6Testing not done (n.d.) due to small number of events.

698 *Eosinophilia noted in one of the samples with lymphocytosis. **Eosinophilia noted in
699 isolation in one case and in another sample with neutrophilia. †One patient received
700 both pre-bronchoscopy antibiotics and post-bronchoscopy antivirals.
701
702 **Supp Table 4. Change in immunosuppression in patients with and without ≥ 7.8%**
703 **$CD57^+PD1^+$ T cells in the $CD4^+$ T cell compartment of at least one BAL**
704 **sample.** Fisher's exact tests were performed. ATG, anti-thymocyte globulin.
705
706 **Supp Table 5. Statistical analysis in patients with and without ≥ 7.8% $CD57^+PD1^+$**
707 **T cells in the $CD4^+$ T cell.**
708
709 **Supp Table 6. Antibody panel for IMC.**
710
711 **Supp Table 7. Antibody panel for CITE-seq.**

References

1 Ali, J. M., Bolton, E. M., Bradley, J. A. & Pettigrew, G. J. Allorecognition pathways in transplant rejection and tolerance. *Transplantation* **96**, 681-688, doi:10.1097/TP.0b013e31829853ce (2013).

2 Chambers, D. C. *et al.* The International Thoracic Organ Transplant Registry of the International Society for Heart and Lung Transplantation: Thirty-eighth adult lung transplantation report - 2021; Focus on recipient characteristics. *J Heart Lung Transplant* **40**, 1060-1072, doi:10.1016/j.healun.2021.07.021 (2021).

3 Kawashima, M. & Juvet, S. C. The role of innate immunity in the long-term outcome of lung transplantation. *Ann Transl Med* **8**, 412, doi:10.21037/atm.2020.03.20 (2020).

4 Bando, K. *et al.* Obliterative bronchiolitis after lung and heart-lung transplantation. An analysis of risk factors and management. *The Journal of thoracic and cardiovascular surgery* **110**, 4-13; discussion 13-14 (1995).

5 Heng, D. *et al.* Bronchiolitis obliterans syndrome: incidence, natural history, prognosis, and risk factors. *J Heart Lung Transplant* **17**, 1255-1263 (1998).

6 Moshkelgosha, S. *et al.* Interferon-stimulated and metallothionein-expressing macrophages are associated with acute and chronic allograft dysfunction after lung transplantation. *J Heart Lung Transplant* **41**, 1556-1569, doi:10.1016/j.healun.2022.05.005 (2022).

7 Bhorade, S. M. *et al.* Interobserver variability in grading transbronchial lung biopsy specimens after lung transplantation. *Chest* **143**, 1717-1724, doi:10.1378/chest.12-2107 (2013).

8 Stephenson, A. *et al.* Interpretation of transbronchial lung biopsies from lung transplant recipients: inter- and intraobserver agreement. *Can Respir J* **12**, 75-77 (2005).

9 Levy, L. *et al.* in *International Society for Heart and Lung Transplantation 39th Annual Meeting* Vol. 38(S4) S163-164 (J Heart Lung Transplant, Orlando FL USA, 2019).

10 Levy, L. *et al.* Epithelial cell death markers in bronchoalveolar lavage correlate with chronic lung allograft dysfunction subtypes and survival in lung transplant recipients-a single-center retrospective cohort study. *Transpl Int* **32**, 965-973, doi:10.1111/tri.13444 (2019).

11 Moshkelgosha, S. *et al.* in *J Heart Lung Transpl* Vol. 37 S216 (2018).

12 Moshkelgosha, S. *et al.* in *International Society for Heart and Lung Transplantation* Vol. 38 S17 (Orlando, FL USA, 2019).

13 Moshkelgosha, S. *et al.* in *J Heart Lung Transpl* Vol. 39 S199-S200 (2020).

14 Whitehead, B. F. *et al.* Analysis of bronchoalveolar lavage from human lung transplant recipients by flow cytometry. *Respiratory medicine* **89**, 27-34 (1995).

15 Reynaud-Gaubert, M. *et al.* Clinical utility of bronchoalveolar lavage cell phenotype analyses in the postoperative monitoring of lung transplant recipients. *European journal of cardio-thoracic surgery : official journal of the European Association for Cardio-thoracic Surgery* **21**, 60-66 (2002).

16 Hodge, S. *et al.* Increased levels of T cell granzyme b in bronchiolitis obliterans syndrome are not suppressed adequately by current immunosuppressive regimens. *Clinical and experimental immunology* **158**, 230-236, doi:10.1111/j.1365-2249.2009.04008.x (2009).

17 Neujahr, D. C. *et al.* Dynamics of human regulatory T cells in lung lavages of lung transplant recipients. *Transplantation* **88**, 521-527, doi:10.1097/TP.0b013e3181b0e719 (2009).
18 Hodge, S. J., Hodge, G. L., Reynolds, P. N. & Holmes, M. D. Differential rates of apoptosis in bronchoalveolar lavage and blood of lung transplant patients. *J Heart Lung Transplant* **24**, 1305-1314, doi:10.1016/j.healun.2004.10.009 (2005).
19 Greenland, J. R. *et al.* Bronchoalveolar lavage cell immunophenotyping facilitates diagnosis of lung allograft rejection. *Am J Transplant* **14**, 831-840, doi:10.1111/ajt.12630 (2014).
20 Bandura, D. R. *et al.* Mass cytometry: technique for real time single cell multitarget immunoassay based on inductively coupled plasma time-of-flight mass spectrometry. *Analytical chemistry* **81**, 6813-6822, doi:10.1021/ac901049w (2009).
21 Van Gassen, S. *et al.* FlowSOM: Using self-organizing maps for visualization and interpretation of cytometry data. *Cytometry A* **87**, 636-645, doi:10.1002/cyto.a.22625 (2015).
22 Bruggner, R. V., Bodenmiller, B., Dill, D. L., Tibshirani, R. J. & Nolan, G. P. Automated identification of stratifying signatures in cellular subpopulations. *Proc Natl Acad Sci U S A* **111**, E2770-2777, doi:10.1073/pnas.1408792111 (2014).
23 Nowicka, M. *et al.* CyTOF workflow: differential discovery in high-throughput high-dimensional cytometry datasets. *F1000Res* **6**, 748, doi:10.12688/f1000research.11622.2 (2017).
24 Tikkanen, J. M. *et al.* De Novo DQ Donor-Specific Antibodies Are Associated with Chronic Lung Allograft Dysfunction after Lung Transplantation. *American journal of respiratory and critical care medicine* **194**, 596-606, doi:10.1164/rccm.201509-1857OC (2016).
25 Renaud-Picard, B. *et al.* in *J Heart Lung Transpl* Vol. 41 S106 (2022).
26 Giesen, C. *et al.* Highly multiplexed imaging of tumor tissues with subcellular resolution by mass cytometry. *Nature methods* **11**, 417-422, doi:10.1038/nmeth.2869 (2014).
27 Watanabe, T. *et al.* A B cell-dependent pathway drives chronic lung allograft rejection after ischemia-reperfusion injury in mice. *American journal of transplantation : official journal of the American Society of Transplantation and the American Society of Transplant Surgeons* **19**, 3377-3389, doi:10.1111/ajt.15550 (2019).
28 Martinu, T. *et al.* Spectrum of chronic lung allograft pathology in a mouse minor-mismatched orthotopic lung transplant model. *Am J Transplant* **19**, 247-258, doi:10.1111/ajt.15167 (2019).
29 Stoeckius, M. *et al.* Simultaneous epitope and transcriptome measurement in single cells. *Nature methods* **14**, 865-868, doi:10.1038/nmeth.4380 (2017).
30 Rao, D. A. *et al.* Pathologically expanded peripheral T helper cell subset drives B cells in rheumatoid arthritis. *Nature* **542**, 110-114, doi:10.1038/nature20810 (2017).
31 Manzo, A. *et al.* Mature antigen-experienced T helper cells synthesize and secrete the B cell chemoattractant CXCL13 in the inflammatory environment of the rheumatoid joint. *Arthritis Rheum* **58**, 3377-3387, doi:10.1002/art.23966 (2008).
32 Huang, Y. *et al.* T peripheral helper cells in autoimmune diseases: What do we know? *Front Immunol* **14**, 1145573, doi:10.3389/fimmu.2023.1145573 (2023).

33 Ng, S. S. *et al.* The NK cell granule protein NKG7 regulates cytotoxic granule exocytosis and inflammation. *Nat Immunol* **21**, 1205-1218, doi:10.1038/s41590-020-0758-6 (2020).
34 Wein, A. N. *et al.* CXCR6 regulates localization of tissue-resident memory CD8 T cells to the airways. *J Exp Med* **216**, 2748-2762, doi:10.1084/jem.20181308 (2019).
35 Milardi, G. *et al.* Follicular helper T cell signature of replicative exhaustion, apoptosis, and senescence in common variable immunodeficiency. *Eur J Immunol* **52**, 1171-1189, doi:10.1002/eji.202149480 (2022).
36 Llao-Cid, L. *et al.* EOMES is essential for antitumor activity of CD8(+) T cells in chronic lymphocytic leukemia. *Leukemia : official journal of the Leukemia Society of America, Leukemia Research Fund, U.K* **35**, 3152-3162, doi:10.1038/s41375-021-01198-1 (2021).
37 Wolf, Y., Anderson, A. C. & Kuchroo, V. K. TIM3 comes of age as an inhibitory receptor. *Nature reviews. Immunology* **20**, 173-185, doi:10.1038/s41577-019-0224-6 (2020).
38 Liu, X., Hoft, D. F. & Peng, G. Senescent T cells within suppressive tumor microenvironments: emerging target for tumor immunotherapy. *J Clin Invest* **130**, 1073-1083, doi:10.1172/JCI133679 (2020).
39 Mittelbrunn, M. & Kroemer, G. Hallmarks of T cell aging. *Nat Immunol* **22**, 687-698, doi:10.1038/s41590-021-00927-z (2021).
40 Hodge, G., Hodge, S., Reynolds, P. N. & Holmes, M. Airway infection in stable lung transplant patients is associated with decreased intracellular T-helper type 1 pro-inflammatory cytokines in bronchoalveolar lavage T-cell subsets. *Transplant infectious disease : an official journal of the Transplantation Society* **10**, 99-105, doi:10.1111/j.1399-3062.2007.00236.x (2008).
41 Hodge, G., Hodge, S., Chambers, D., Reynolds, P. N. & Holmes, M. Acute lung transplant rejection is associated with localized increase in T-cell IFNgamma and TNFalpha proinflammatory cytokines in the airways. *Transplantation* **84**, 1452-1458, doi:10.1097/01.tp.0000290679.94163.e1 (2007).
42 Hodge, G., Hodge, S., Reynolds, P. N. & Holmes, M. Compartmentalization of intracellular proinflammatory cytokines in bronchial intraepithelial T cells of stable lung transplant patients. *Clinical and experimental immunology* **145**, 413-419, doi:10.1111/j.1365-2249.2006.03143.x (2006).
43 Hodge, G., Hodge, S., Reynolds, P. N. & Holmes, M. Increased intracellular pro- and anti-inflammatory cytokines in bronchoalveolar lavage T cells of stable lung transplant patients. *Transplantation* **80**, 1040-1045 (2005).
44 Libri, V. *et al.* Cytomegalovirus infection induces the accumulation of short-lived, multifunctional CD4+CD45RA+CD27+ T cells: the potential involvement of interleukin-7 in this process. *Immunology* **132**, 326-339, doi:10.1111/j.1365-2567.2010.03386.x (2011).
45 Di Mitri, D. *et al.* Reversible senescence in human CD4+CD45RA+CD27- memory T cells. *J Immunol* **187**, 2093-2100, doi:10.4049/jimmunol.1100978 (2011).
46 Martinu, T. *et al.* International Society for Heart and Lung Transplantation consensus statement for the standardization of bronchoalveolar lavage in lung transplantation. *J Heart Lung Transplant*, doi:10.1016/j.healun.2020.07.006 (2020).

47 Amir el, A. D. *et al.* viSNE enables visualization of high dimensional single-cell data and reveals phenotypic heterogeneity of leukemia. *Nat Biotechnol* **31**, 545-552, doi:10.1038/nbt.2594 (2013).
48 Schapiro, D. *et al.* histoCAT: analysis of cell phenotypes and interactions in multiplex image cytometry data. *Nat Methods* **14**, 873-876, doi:10.1038/nmeth.4391 (2017).
49 Zheng, G. X. Y. *et al.* Massively parallel digital transcriptional profiling of single cells. *Nature communications* **8**, 14049, doi:10.1038/ncomms14049 (2017).
50 Butler, A., Hoffman, P., Smibert, P., Papalexi, E. & Satija, R. Integrating single-cell transcriptomic data across different conditions, technologies, and species. *Nature biotechnology* **36**, 411-420, doi:10.1038/nbt.4096 (2018).
51 Hafemeister, C. & Satija, R. Normalization and variance stabilization of single-cell RNA-seq data using regularized negative binomial regression. *Genome Biology* **20**, 296, doi:10.1186/s13059-019-1874-1 (2019).
52 La Manno, G. *et al.* RNA velocity of single cells. *Nature* **560**, 494-498, doi:10.1038/s41586-018-0414-6 (2018).
53 Bergen, V., Lange, M., Peidli, S., Wolf, F. A. & Theis, F. J. Generalizing RNA velocity to transient cell states through dynamical modeling. *Nature biotechnology* **38**, 1408-1414, doi:10.1038/s41587-020-0591-3 (2020).
54 Katz, G. & Snow, A. L. Fluorescence-activated cell sorting-based quantitation of T cell receptor restimulation-induced cell death in activated, primary human T cells. *Methods Mol Biol* **979**, 15-23, doi:10.1007/978-1-62703-290-2_2 (2013).
712

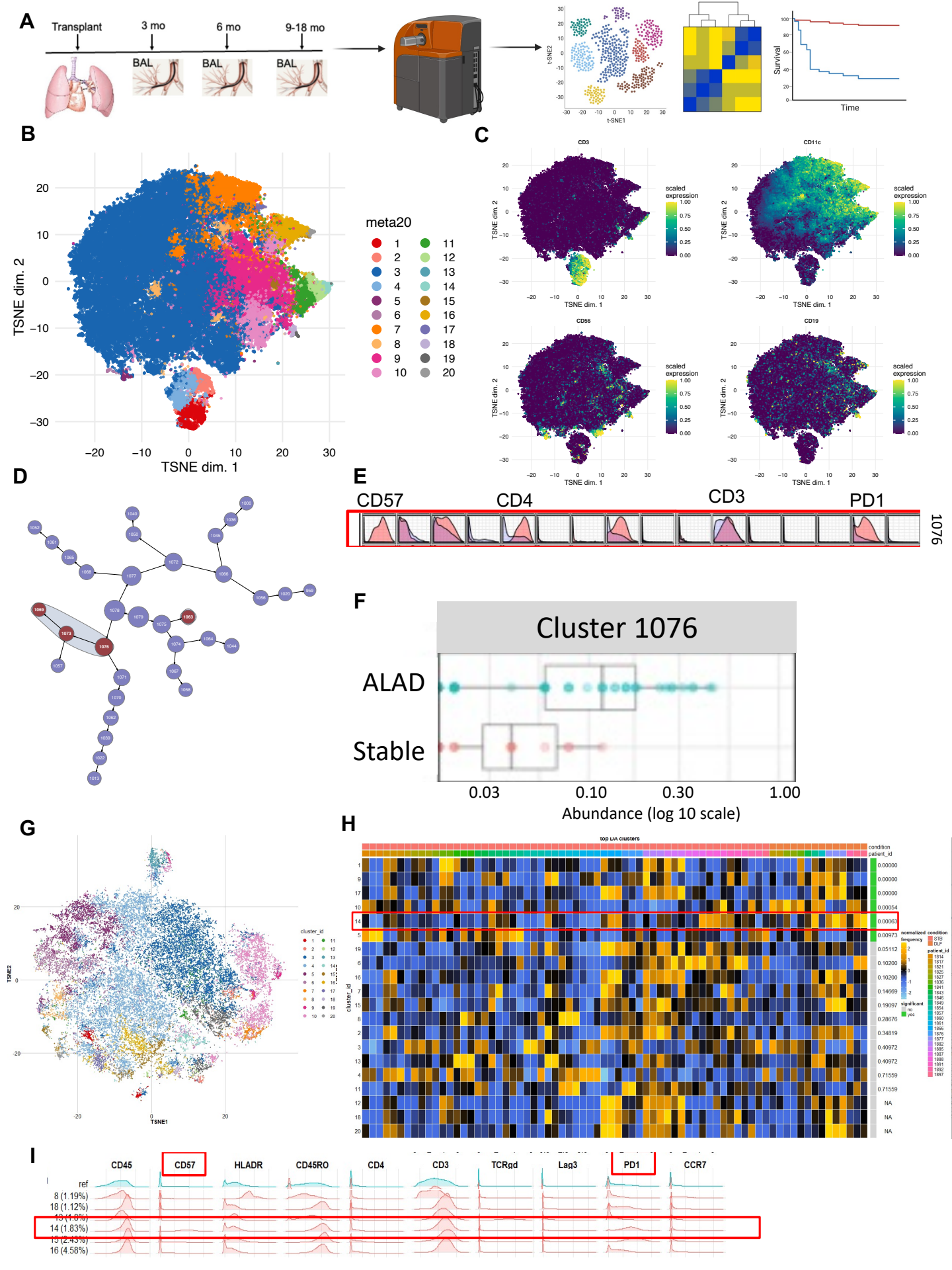
A
Transplant
3 mo
6 mo
9-18 mo
BAL
BAL
BAL
t-SNE2
t-SNE1
Survival
Time
B
TSNE dim. 2
TSNE dim. 1
meta20
1
2
3
4
5
6
7
8
9
10
11
12
13
14
15
16
17
18
19
20
C
CD3
CD11c
CD56
CD19
scaled expression
TSNE dim. 1
TSNE dim. 2
D
E
CD57
CD4
CD3
PD1
1076
F
Cluster 1076
ALAD
Stable
0.03
0.10
0.30
1.00
Abundance (log 10 scale)
G
cluster_id
TSNE1
TSNE2
H
top DA clusters
condition
patient_id
normalized frequency
significant
I
CD45
CD57
HLADR
CD45RO
CD4
CD3
TCRgd
Lag3
PD1
CCR7
ref
8 (1.19%)
18 (1.12%)
14 (1.83%)
16 (4.58%)

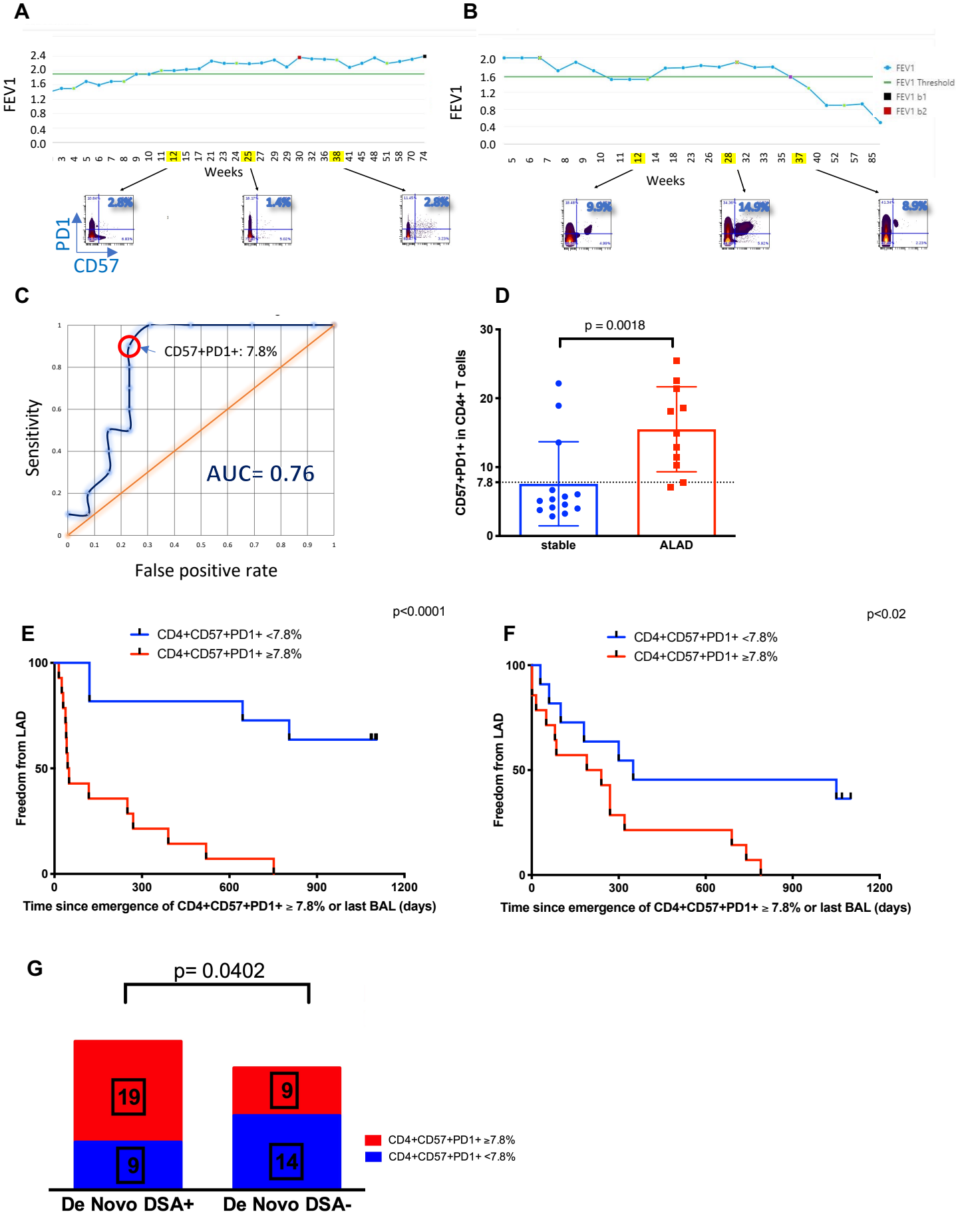
A
FEV1
Weeks
PD1
CD57
2.6%
1.4%
2.6%
B
FEV1
FEV1 Threshold
FEV1 b1
FEV1 b2
Weeks
9.9%
14.9%
8.9%
C
CD57+PD1+: 7.8%
AUC= 0.76
Sensitivity
False positive rate
D
p = 0.0018
CD57+PD1+ in CD4+ T cells
stable
ALAD
E
p<0.0001
CD4+CD57+PD1+ <7.8%
CD4+CD57+PD1+ ≥7.8%
Freedom from LAD
Time since emergence of CD4+CD57+PD1+ ≥ 7.8% or last BAL (days)
F
p<0.02
CD4+CD57+PD1+ <7.8%
CD4+CD57+PD1+ ≥7.8%
Freedom from LAD
Time since emergence of CD4+CD57+PD1+ ≥ 7.8% or last BAL (days)
G
p= 0.0402
19
9
9
14
CD4+CD57+PD1+ ≥7.8%
CD4+CD57+PD1+ <7.8%
De Novo DSA+
De Novo DSA-

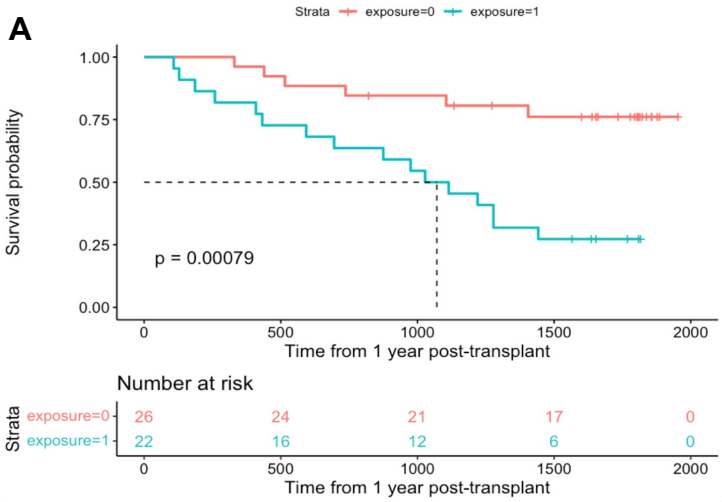
A
Strata
exposure=0
exposure=1
Survival probability
1.00
0.75
0.50
0.25
0.00
p = 0.00079
0
500
1000
1500
2000
Time from 1 year post-transplant
Number at risk
Strata
exposure=0 26 24 21 17 0
exposure=1 22 16 12 6 0
Time from 1 year post-transplant

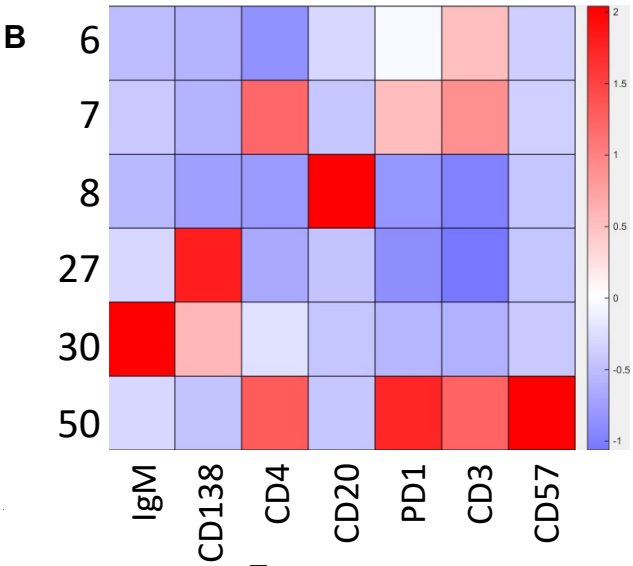
B
6
7
8
27
30
50
IgM
CD138
CD4
CD20
PD1
CD3
CD57
2
1.5
1
0.5
0
-0.5
-1

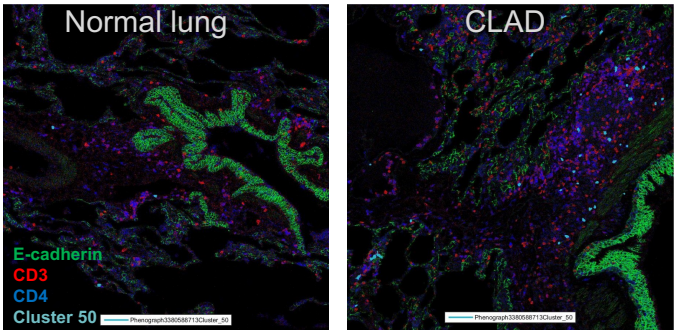
C
Normal lung
CLAD
E-cadherin
CD3
CD4
Cluster 50

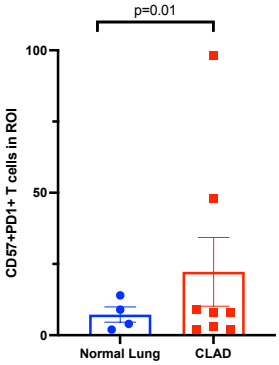
D
p=0.01
CD57+PD1+ T cells in ROI
100
50
0
Normal Lung
CLAD

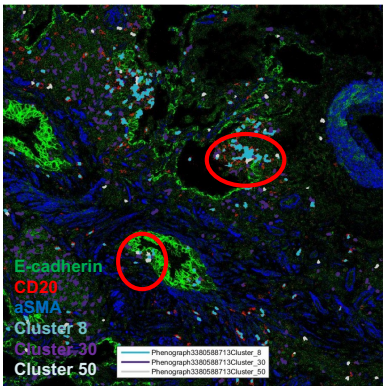
E
E-cadherin
CD20
aSMA
Cluster 8
Cluster 30
Cluster 50

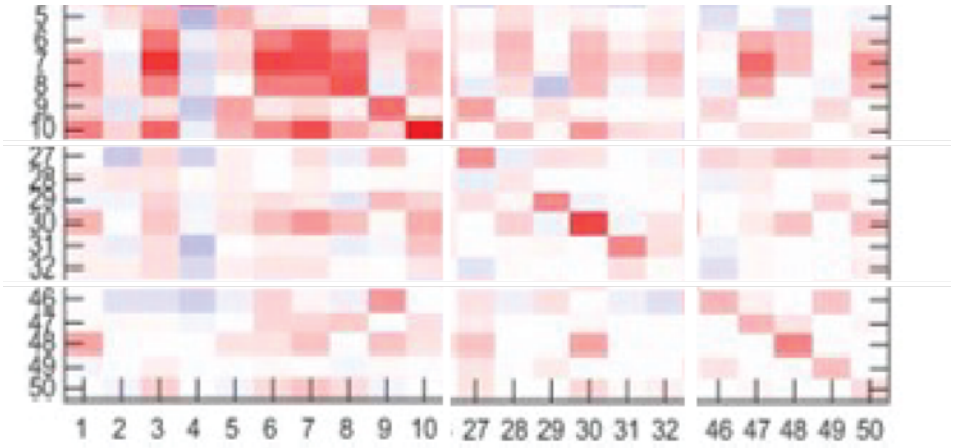
F
1 2 3 4 5 6 7 8 9 10
27 28 29 30 31 32
46 47 48 49 50

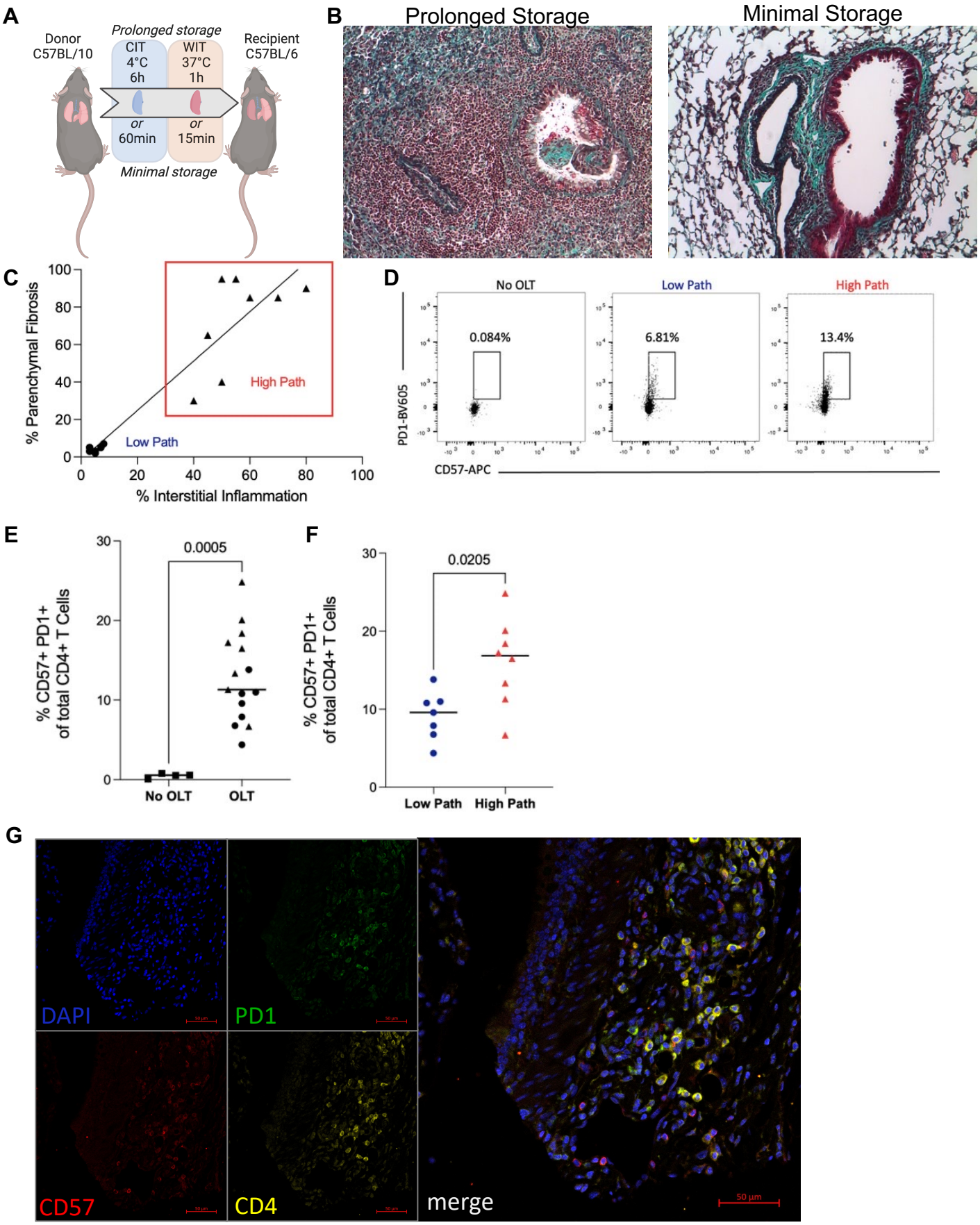
A
Donor
C57BL/10
Prolonged storage
CIT
4°C
6h
WIT
37°C
1h
Recipient
C57BL/6
or
60min
or
15min
Minimal storage
B
Prolonged Storage
Minimal Storage
C
% Parenchymal Fibrosis
% Interstitial Inflammation
High Path
Low Path
D
No OLT
Low Path
High Path
0.084%
6.81%
13.4%
PD1-BV605
CD57-APC
E
0.0005
% CD57+ PD1+ of total CD4+ T Cells
No OLT
OLT
F
0.0205
% CD57+ PD1+ of total CD4+ T Cells
Low Path
High Path
G
DAPI
PD1
CD57
CD4
merge
50 µm

Figure 5

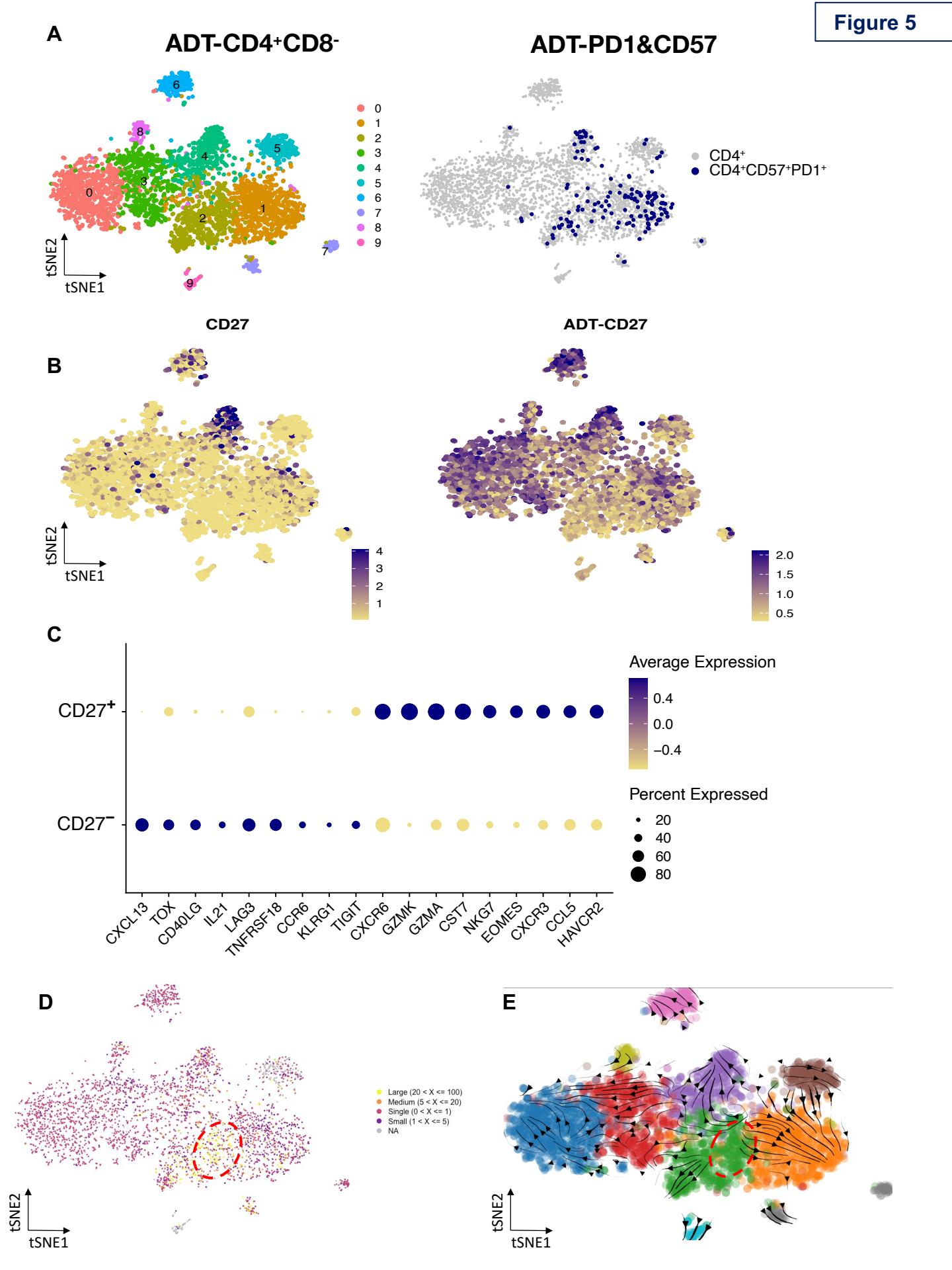
A
ADT-CD4+CD8-
ADT-PD1&CD57
0
1
2
3
4
5
6
7
8
9
tSNE2
tSNE1
CD4+
CD4+CD57+PD1+
B
CD27
ADT-CD27
4
3
2
1
2.0
1.5
1.0
0.5
C
CD27+
CD27−
Average Expression
0.4
0.0
−0.4
Percent Expressed
20
40
60
80
CXCL13
TOX
CD40LG
IL21
LAG3
TNFRSF18
CCR6
KLRG1
TIGIT
CXCR6
GZMK
GZMA
CST7
NKG7
EOMES
CXCR3
CCL5
HAVCR2
D
Large (20 < X <= 100)
Medium (5 < X <= 20)
Single (0 < X <= 1)
Small (1 < X <= 5)
NA
E

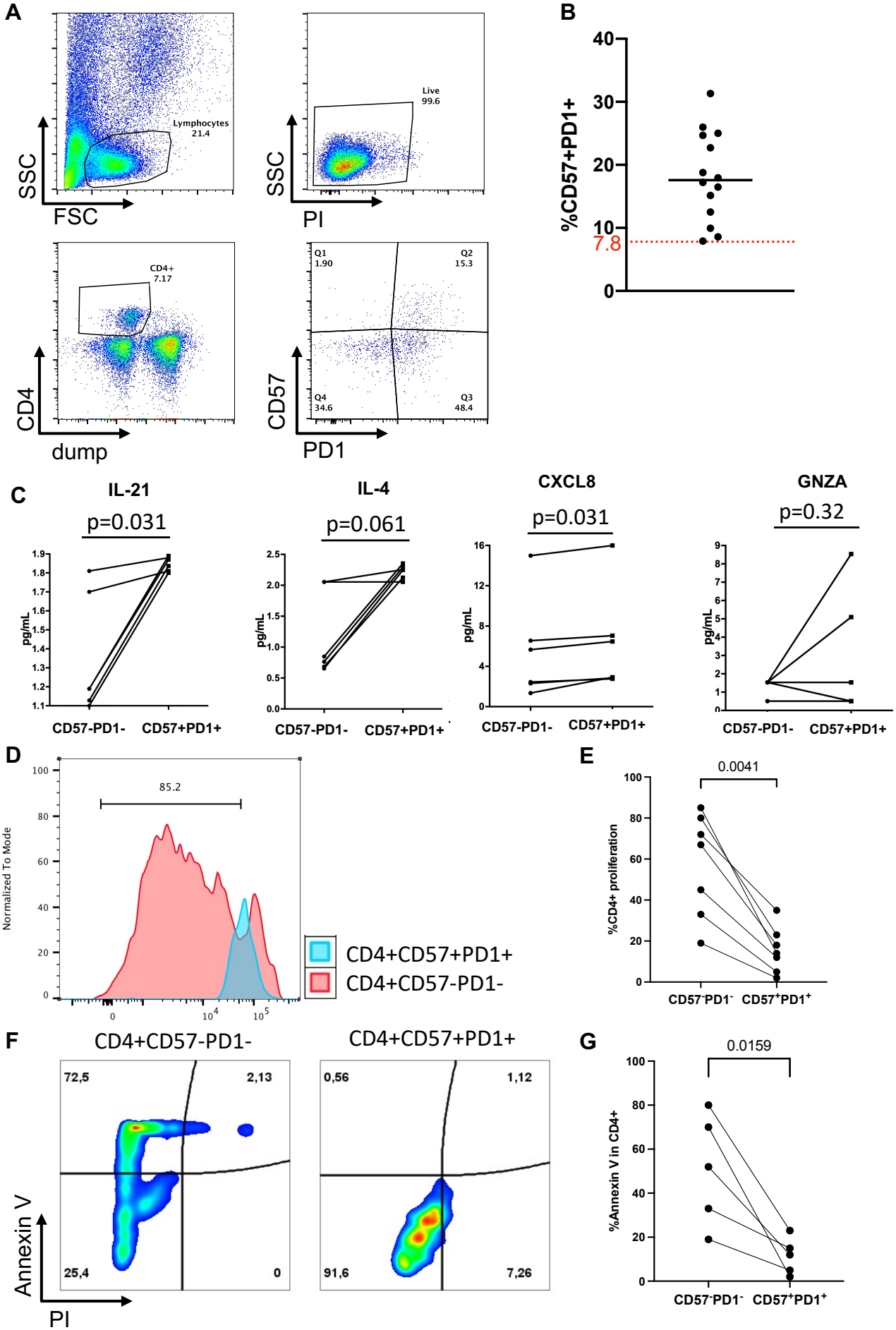
A
Lymphocytes
21.4
SSC
FSC
Live
99.6
SSC
PI
CD4+
7.17
CD4
dump
Q1
1.90
Q2
15.3
Q4
34.6
Q3
48.4
CD57
PD1
B
%CD57+PD1+
40
30
20
10
7.8
0
C
IL-21
p=0.031
IL-4
p=0.061
CXCL8
p=0.031
GNZA
p=0.32
pg/mL
CD57-PD1-
CD57+PD1+
D
85.2
Normalized To Mode
CD4+CD57+PD1+
CD4+CD57-PD1-
E
0.0041
%CD4+ proliferation
CD57-PD1-
CD57+PD1+
F
CD4+CD57-PD1-
CD4+CD57+PD1+
72,5
2,13
25,4
0
0,56
1,12
91,6
7,26
Annexin V
PI
G
0.0159
%Annexin V in CD4+
CD57-PD1-
CD57+PD1+